Black Hole Horizons During Extreme Mass Ratio Mergers

by

© *Saikat Mondal*

Mun ID- 201891324

A thesis submitted to the

School of Graduate Studies

in partial fulfilment of the

requirements for the degree of

Master of Science

Department of Physics and Physical Oceanography

Memorial University of Newfoundland

September 2020

St. John's Newfoundland

Abstract

A marginally outer trapped surface (MOTS) is a quasi-local alternative to the event horizon that captures the dynamical features of a black hole. Previously, Emparan and Martínez have shown that the evolution of the event horizon during extreme mass ratio (EMR) mergers can be solved exactly in the limit where the large black hole becomes infinite in extent. In this project, we studied the evolution of MOTS during EMR mergers in the same setup where MOTS can be locally approximated by spacelike open surfaces with vanishing null expansion in the Schwarzschild geometry. We defined these open surfaces as marginally outer trapped open surfaces (MOTOS), which can be fully determined by the local properties of spacetime. We studied axisymmetric MOTOS contained in constant time slices of Schwarzschild spacetimes in different coordinate systems. In the Painlevé-Gullstrand coordinate system, we found open and closed surfaces with an arbitrary number of self-intersections inside the Schwarzschild horizon. We also extrapolate these results to predict possible behaviours of MOTS during extreme mass ratio mergers based on previous numerical studies of the evolution of MOTS during black hole mergers.

Statement of Contribution

I, Saikat Mondal (SM) hereby declare that this thesis manuscript is entirely my own. The work presented in it is done by myself together with Dr. Ivan Booth (IB) and Dr. Robie Hennigar (RH). The theoretical work can be divided in four parts. First, in chapter 3, I reproduced the figures obtained by Emparan and Martínez [17] by solving the problem of evolution of event horizon during EMR mergers, numerically with the help of RH. Next, the study of MOTOS in Schwarzschild geometry is done in three different coordinate systems. The computations in isotropic cylindrical coordinates is performed by SM with RH provided critical feedback and helped shape the analysis. The study of these surfaces in Schwarzschild standard coordinates is devised and carried out by IB and verified by SM. The most crucial part of the work that is investigation of MOTOS in Painlevé-Gullstrand coordinates is written based on the article [13], "MOTS in Schwarzschild: multiple self-intersections and extreme mass ratio mergers", authored by IB, RH and SM.

General Summary

With likely billions of them existing in the universe, black holes are common astrophysical objects. Black holes form the core of most galaxies, and their collisions represent one of the most dramatic phenomena in the universe. Generally, a detailed study of black holes involves solving complex differential equations which require heavy computational resources. In this project, we studied the evolution of black holes during a special kind of black hole merger: an extreme mass ratio merger, where one of the black holes is much larger than the other. A physical example would be a supermassive black hole hole swallowing a stellar mass one. In this case the merging black holes can be studied with simple laptop numerics rather than supercomputers.

A defining feature of a black hole is its horizon, which is the boundary which marks the point of no escape. There are many different ways to describe black hole horizons, and here our focus was marginally outer trapped surfaces. Our objective was to understand the fusion of these horizons during a black hole merger. Along the way, we also uncovered a novel class of marginally outer trapped surfaces characterized by an arbitrary number of self-intersections.

Acknowledgements

I would like to express my gratitude to my supervisor Dr. Ivan Booth for his guidance during my Master's thesis work. He has always given me encouragement whenever I needed it. I could not have imagined having a better supervisor and mentor for my masters study. I am grateful to Dr. Robie Hennigar for his advice and support at every step during the thesis work. Without their help, finishing this thesis would have been a distant dream.

I am thankful to all the members of Gravity group journal club-specially Turkuler Durgut, Sharmin Rahi for the wonderful memories together.

I would like to thank Natural Science and Engineering Research Council of Canada and School of Graduate studies for their financial support.

Finally, I would like to acknowledge with gratitude, the support and love of my parents, my sisters and Ahana. They all kept me going and help me getting through the tough times during this project.

"Black holes are where God divided by zero."

— Albert Einstein

Contents

List of Figures

Chapter 1

Introduction

Black holes are one of the central objects in astrophysics. Though indirect evidence has confirmed the existence of black holes for the last few decades, it has only been during the last five years we have been able to observe these objects directly through gravitational wave detectors. However, the idea of an enigmatic, invisible object that traps light was there since the late 18th century. John Michell [37] and Pierre-Simon Laplace [34] predicted the existence of very dense “dark stars” that trap light by calculating the escape velocity of light using Newton’s gravitational laws. But this concept was dropped when it was discovered that light is a wave [38] in the beginning of the 19th century.

After almost a century, the particle theory of light was rejuvenated by Albert Einstein. In 1905, he published a paper [16] proposing that light energy is carried in discrete quantized packets (called photons) in order to explain the photoelectric effect. He believed that a wave of light is nothing but a flow of photons. A decade later he published the famous theory of general relativity [48] where he explained the behaviour of light under gravity.

Just one year after the general theory of relativity was published, Karl Schwarzschild obtained a vacuum solution [51] to the Einstein field equations. The Schwarzschild solution has a singularity at its origin where the curvature blows up. It also predicted the existence of a critical radius, which light rays are unable to cross from inside. This is known as the Schwarzschild radius. Schwarzschild's solution is the prototypical example of a black hole, and the hypersurface corresponding to the Schwarzschild radius is known as the event horizon[1] as it keeps the events inside it from influencing events outside. Other solutions of Einstein field equations (e.g. spacetimes belonging to the Kerr-Newman family) also have curvature singularities and horizons. The initial concept of a black hole consisted of the singularity and the event horizon(s). However, this characterization of a black hole has a few complications.

First of all, there is no theorem that tells us that the singularities that arise in the solutions of the Einstein field equations (subjected to certain physical requirements) are always hidden inside an event horizon. A singularity that is not covered by a horizon is known as naked singularity. Naked singularities can be observed from the rest of the spacetime. This is not feasible as the physical behaviour of singularities is unpredictable and causality may break down. To avoid this inconsistency, Roger Penrose proposed the cosmic censorship conjectures [43] in 1969. The weak cosmic censorship conjecture states that in an asymptotically flat spacetime any singularity will be hidden from infinity by an event horizon and that a black hole will form. This hypothesis is yet to be proven.

Secondly, the event horizon is defined as the boundary of the casual past of fu-

[1]The term "black hole" was first coined by John Wheeler much later in 1967 [30].

ture null infinity. Because of this non-local definition, the study of an event horizon requires the knowledge of the global causal structure. It is a teleological characterization of a black hole boundary which depends on the final fate of null curves. By construction, it also means that event horizons are only defined for spacetimes that have a future null infinity. Moreover, even for a spacetime with a future null infinity, we have to wait till the very "end of time" in order to locate the event horizon.

From the above discussion, it is clear that for highly dynamical situations that depend only on the local properties of spacetime, the event horizon is not very useful [40, 8, 4]. There are alternative characterizations of a black hole which are both physical and local. Here in this project, we will focus on one of these concepts: trapped surfaces. Trapped (or closed trapped) surfaces were defined by Roger Penrose [42] in order to describe the inner region of black holes. Heuristically,[2] trapped surfaces are spacelike two dimensional surfaces with the property that their area decreases locally along any possible future null direction [9] in a four dimensional spacetime. The definition and the classification of trapped surfaces are discussed in [53] in detail. Black hole solutions of the Einstein field equations that belong to the Kerr-Newman family possess closed trapped surfaces and all these surfaces are inside the event horizon [58, 29].

In 1965, Penrose [42] demonstrated that, if a spacetime contains a trapped surface, the null energy condition holds and there is a non-compact Cauchy surface for the spacetime, then this spacetime contains a singularity. Based on this idea, Penrose and Stephen Hawking then established a number of singularity theorems [29, 28, 44, 52]. A key ingredient of these singularity theorems is the existence of a closed trapped

[2]The rigorous definition of trapped surfaces is given in the next chapter.

surface. This provides a strong argument for trapped surfaces being fundamental to the existence of black holes. Moreover, a practical notion of the “horizon” can be identified with the boundary of the spacetime region containing trapped surfaces. The boundary of the region that contains the trapped surface separates the trapped surfaces from surfaces which are not trapped. This general notion can be understood easily for a specific case: the Schwarzschild black hole. In this prototypical example of a black hole, all the trapped surfaces are located inside the event horizon, while the surfaces outside are not trapped. Here the former ones are being trapped in the sense that their area decreases along any future direction. Therefore it suggests that there should be a boundary between being trapped and not being trapped which is a special and useful characterization of the black hole. It also gives an indication that the boundary should be a surface with its area remaining unchanged along any future direction.

This intuition is formalized in the definition of marginally trapped outer surfaces (MOTS). A MOTS is a closed spacelike surface such that the expansion in the direction of the outgoing null normal vanishes. Heuristically, the expansion scalar in this definition can be understood as describing the rate of change of area for a two dimensional surface, and so MOTS represent those surfaces for which the area remains unchanged along the outgoing future null direction. Spacelike slices of all horizons (including cosmological horizons) in spacetimes belonging to the Kerr-Newman family are MOTS.

MOTS can be understood as the boundary of a trapped region of a spacetime, i.e. a quasi-local boundary of a black hole. It is better suited as an alternative to the event horizon for studying dynamical aspects of black holes [12, 49, 50, 4, 25, 6, 10]. Black holes play a crucial role in modelling of astrophysical systems. In fact, understanding the detailed dynamics of black holes in astrophysical situations is becoming increasingly important due to modern high-precision experiments. Due to its complexity, these dynamical black hole situations (e.g. gravitational collapse) are studied numerically. The numerical methods used in these situations deal with finite space and time. In these cases, the concept of event horizon is not the most useful tool. For the last few decades, MOTS/apparent horizons have been identified as the boundary of a black hole in practice for numerical studies [57, 7, 56, 15, 11].

Using MOTS to understand horizon evolution during black hole mergers has a long history [5, 50, 56, 33, 3, 39, 26, 47, 46, 23]. An exciting new development in this area is the result of [39] where it was demonstrated that the individual MOTSs approach and penetrate each other during the merger of a small and a big black hole. However, due to numerical limitations this work leaves open the question of what happens after the self-intersection occurs. In [47, 46], they used the stability parameter to predict the behaviour of MOTS during a merger. They have identified self-intersecting MOTS after the black holes started to merge together. In this project we strive to learn the behaviours of MOTS in order to understand a specific case of black hole mergers, that is extreme mass ratio mergers.

In the case of an extreme mass ratio merger (EMR), one black hole is much greater in size than the other. A physical case of such a merger would be a supermassive black hole merging with a small stellar black hole. There are two perspectives from which EMR mergers can be considered. In the first case, as studied in [27, 32], the focus is on the dynamics at the scale of the large black hole. The other perspective is to focus on the dynamics at the scale of the small black hole. Both perspectives yield useful information, but it is the latter approach that will be the focus of this thesis.

For an extreme mass ratio merger of non-rotating black holes where we are working on the small black hole length scale, the problem reduces to an analytical one with the help of the equivalence principle. The horizon of the large black hole can be approximated as a null planar surface when the small black hole is very close to the large black hole. Also the spacetime around the small black hole can be approximated as the Schwarzschild spacetime locally with a condition that the event horizon here is a null hypersurface that reaches future null infinity at a finite retarded time. This is different than the event horizon of the Schwarzschild spacetime at $r = 2m$, which is a null hypersurface that reaches future null infinity an infinite retarded time. The idea behind this approximation is that the event horizon for the fall of an object into an acceleration horizon can be obtained by tracing an appropriate family of light rays in the spacetime of that object. This idea is used by several other studies [1, 24, 19, 55]. Note that these local approximations are only valid near the small black hole. This EMR limit is brilliantly employed by Emparan and Martínez to study evolutions of event horizon for extreme mass ratio black hole mergers [17, 18] and later neutron star-black hole mergers [20].

A more complex problem is to study the evolution of MOTS during extreme mass ratio mergers. Our original motivation for this project was to study MOTS as an extension of [17, 18]. In the same setup, it is not unreasonable to expect that open spacelike two dimensional surfaces with vanishing outward null expansion can be a local approximation to MOTS of the large black hole. This is similar to the fact that in this setup the event horizon of the large black hole is approximated by a null planar surface. Closure depends on the far-away geometry of the spacetime. It is not feasible to determine whether a surface is closed or not when we focus on the local geometry. We label these open surfaces with vanishing outward null expansion to be marginally outer trapped *open* surfaces (MOTOS).

In this project, we studied axisymmetric MOTOS in the Schwarzschild geometry and tried to build an understanding of the general behaviour of MOTS. To do this, we need to identify the correct MOTOS that represents the "actual" geometric horizon. We provide partial results towards this. Among the different axisymmetric MOT(O)S [3] we have found an infinite family of self-intersecting MOT(O)S. With these results we not only able to study the behaviours of MOTS seen in [47, 46], but also speculate on new behaviours in the aftermath of a merger.

The structure of the thesis is as follows. In the next chapter, we go through basic concepts like null congruences, expansion scalar, null hypersurface and derive the equations of light rays in the Schwarzschild geometry. We also review different black hole boundaries: event horizon, trapped surfaces, apparent horizon in the chapter. Then we move on to discuss event horizons during an extreme mass ratio black hole merger in chapter 3. There we will review the work done by Emparan and Martínez [17]. Whereas they have solved the problem exactly, we will present similar figures as a result of our numerical calculation. Chapter 4 talks about MOTOS in the Schwarzschild geometry in three different coordinate systems namely, Schwarzschild standard coordinates, isotropic cylindrical coordinates and Painlevé-Gullstrand (PG) coordinates. In all these three coordinate systems, we first set up the problem and derived the partial differential equation for axisymmetric MOTOS. Then we try to learn as much as possible about the MOTOS analytically by employing perturbative

[3] Here MOT(O)S indicates either MOTS or MOTOS.

methods. Later we solve the MOTOS equation numerically and present the resulting figures. In the Schwarzschild standard coordinate system and isotropic cylindrical coordinate system, the behaviour of MOTOS are qualitatively similar, whereas in PG coordinates, more interesting behaviours are observed. There are fully-fledged MOTS inside $r = 2m$ with arbitrary number of self-intersections. We tried to work through the possible solutions systematically and examine any possible insights that are useful to the general behaviour of MOTS in extreme mass ratio mergers. In the last chapter, we conclude this thesis by summarising the results and by discussing the possible future works.

Chapter 2

Basic Concepts

In this section, we introduce the basic concepts and tools that will help us to understand more complex ideas that are presented in the later chapters. Much of the discussion here is based on [45, 58].

2.1 Null Geodesics and Expansion Scalar

A geodesic generalizes the idea of the shortest possible path between two points. In tensor algebra, it is defined as a special curve parameterized by λ, satisfying

$$t^\mu \nabla_\mu t^\alpha \propto t^\alpha \tag{2.1}$$

$$\implies t^\mu \nabla_\mu t^\alpha = \kappa(\lambda) t^\alpha \,, \tag{2.2}$$

where $t^\mu \equiv \mathrm{d}x^\mu/\mathrm{d}\lambda$ is the tangent vector of the curve and $\kappa(\lambda)$ is an inaffiniity parameter. A parameter s for which κ vanishes, i.e. $\kappa(s) = 0$, is known as an affine parameter. All affine parameters are linear multiples of each other. That is for any two affine parameters s and s', $s' = \delta s + s_o$ for some $\delta, s_o \in \mathbb{R}$. For the rest of this chapter, we will assume geodesics are parameterized by affine parameter. Now, geodesics are classified into three types: timelike, spacelike and null. Null geodesics are those geodesics that have a null tangent vector, i.e. $t^\mu t_\mu = 0$.

A congruence of null geodesics in a region N is a family of null geodesics such that there is only one null geodesic from the family that passes through each point of N. Consider a congruence of null geodesics with tangent k^α. The transverse space for a null congruence is essentially a two dimensional space. The reason is that the null vector is orthogonal to itself so distance along the congruence is zero. For example, consider Minkowski spacetime for which the metric ($\mathrm{d}s^2 = -\mathrm{d}t^2 + \mathrm{d}x^2 + \mathrm{d}y^2 + \mathrm{d}z^2$) in a new coordinate system (v,u,θ, ϕ) takes the form,

$$\mathrm{d}s^2 = -\mathrm{d}u\mathrm{d}v + \mathrm{d}y^2 + \mathrm{d}z^2 \tag{2.3}$$

where $u = t - x$ and $v = t + x$ are the new null coordinates. It can be seen that for null curves that have $u =$ constant, the transverse metric becomes two dimensional, $\mathrm{d}\hat{s}^2 = \mathrm{d}y^2 + \mathrm{d}z^2$.

A null direction always has an auxiliary null direction associated with it. For a null vector k^α, the auxiliary null vector N^β can be chosen such that $k^\alpha N_\alpha = -1$. For a given null vector k^α and auxiliary null vector N^β, the transverse metric is,

$$q_{\alpha\beta} = g_{\alpha\beta} + k_\alpha N_\beta + N_\alpha k_\beta \,, \tag{2.4}$$

where $g_{\alpha\beta}$ is the spacetime metric. Now the expansion scalar for the congruence is,

$$\theta = q^{\alpha\beta}\nabla_\beta k_\alpha \,. \tag{2.5}$$

The expansion scalar here tells us whether the null geodesics will converge or move away from each other. Now, if we consider a two dimensional surface in the transverse space of the congruence, then the tangent vector k^α will be normal to the surface. Also the induced metric on the two dimensional surface will be the transverse metric expressed in surface coordinates,

$$q_{AB} = q_{\alpha\beta} e^\alpha_A e^\beta_B \,, \tag{2.6}$$

where e^α_A are the push-forward/pull-back operators between the metric on the space-time and on the surface. Similarly, the expansion scalar for the surface that determines the expansion of the area of the surface, is the same as the expansion scalar of the congruence,

$$\theta = q^{AB} \nabla_B k_A = q^{\alpha\beta} \nabla_\beta k_\alpha \,. \tag{2.7}$$

2.2 Event Horizon

The most defining characteristic of a black hole is its event horizon. In the simplest of terms, a black hole is a region from where no signal can ever escape and its boundary is known as an event horizon, which relative to observer at infinity, is an infinite redshift (black) surface and point of no escape (hole).

Let us now build toward the formal definition of a black hole event horizon. Heuristically, one can think of a black hole as a region of space for which the escape velocity is faster than light. As described by general relativity, black holes are perfect absorbers: they take in everything that impinges on them, but emit nothing. Any event that occurs outside of it, is connected to spacetime infinity by causal curves (timelike/null curves). Light rays or any particle that follows these timelike curves end up in a distant region where the gravitational field is negligible. Our interest will be in situations where far from a massive body the spacetime can be approximated as flat, which to a good approximation describes local physics in our universe. If we choose the spacetime to approach Minkowski spacetime in an asymptotic region, then the spacetime is called asymptotically flat spacetime. The difference between the events inside the black hole that are confined and those ones outside the black hole that can escape to infinity where gravity is negligible, is crucial to define the event horizon in an asymptotically flat spacetime.[1] Due to this one needs to know the global causal structure of spacetime, especially the structure of infinity of spacetime to define the event horizon.

The Structure of Infinity in Minkowski Spacetime: Minkowski space does not have any point one can denote as the location of infinity. However, it can be mapped into a finite region, equipped with a boundary. This can be done in many ways, depending on how one maps the neighbourhood of infinity into a finite region.

Since nothing can travel faster than light and all observers agree on the speed of light, the structure of null geodesics in a spacetime provides an invariant structure for the causal relationship between spacetime events. Moreover, since the distance between any two points along a null curve vanishes, i.e. $\mathrm{d}s^2 = 0$ restricted to a null curve, one is free to change the metric by an overall factor — a conformal transformation — without distorting the causal structure of the spacetime. This freedom can be effectively used to obtain simpler, pictorial representations of the spacetime (these are called Penrose diagrams) that preserve the causal relationships between events. Null

[1] However, this is a choice rather than a requirement. Event horizons also can be defined for asymptotically AdS spacetimes.

geodesics can be easily visualized and tracked in a Penrose diagram. The collection of all spacetime events that can send null geodesics to any set of spacetime points is called the "past" of that set.

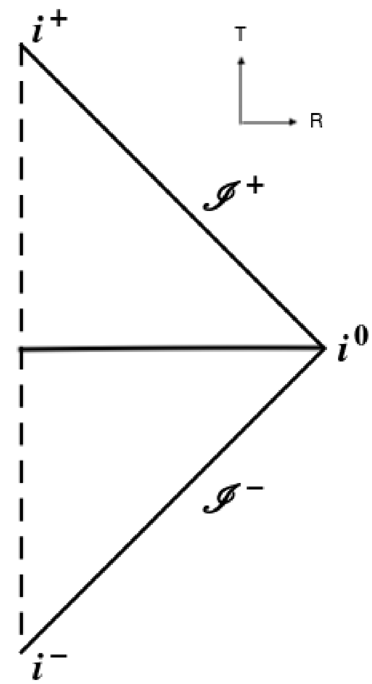

Figure 2.1: Penrose diagram for Minkowski space [41]. Each point represents a two sphere at a fixed radius and a fixed time. Here $i^0 = (0, \pi)$ is spacelike infinity, $i^+ = (\pi, 0)$ is future timelike infinity, $i^- = (-\pi, 0)$ is past timelike infinity, $\mathscr{I}^+$ is future null infinity and $\mathscr{I}^-$ is past null infinity.

As an example, let us consider Minkowski space in spherical coordinates for which the metric reads

$$\mathrm{d}s^2 = -\mathrm{d}t^2 + \mathrm{d}r^2 + r^2\mathrm{d}\theta^2 + r^2\sin^2\theta\mathrm{d}\phi^2\,, \tag{2.8}$$

where $-\infty < t < \infty$, $r > 0$, $0 < \theta < \pi$ and $-\pi < \phi < \pi$. This can be conformally transformed by a change of coordinates from (t,r,θ,ϕ) to (T,R,θ,ϕ) by the transformations

$$R = \arctan(t+r) - \arctan(t-r) \quad \text{and} \quad T = \arctan(t+r) + \arctan(t-r)\,, \tag{2.9}$$

which leads to

$$\mathrm{d}s^2 = \frac{1}{4\cos^2(\frac{T+R}{2})\cos^2(\frac{T-R}{2})}(-\mathrm{d}T + \mathrm{d}R + r^2(R)\mathrm{d}\Omega^2)\,, \tag{2.10}$$

where $\mathrm{d}\Omega^2 = \mathrm{d}\theta^2 + \sin^2\theta \mathrm{d}\phi^2$ and $r^2(R) = \sin^2 R$. Due to the nature of the arctan function, the new coordinates (T, R) range over the half-diamond $R \pm T < \pi$, $R > 0$ and are hence compact. This can be seen in figure 2.1, which shows the Penrose diagram of Minkowski spacetime.

Now, we can define an event horizon formally. For an asymptotically flat spacetime, which in particular has a future null infinity ($\mathscr{I}^+$), the event horizon is defined to be *the boundary of the past of future null infinity* [29]. For the Schwarzschild spacetime, the event horizon can also be understood as a null hypersurface that is orthogonal to the congruence of light rays that reaches $\mathscr{I}^+$ at infinite retarded time [17]. In a D-dimensional spacetime, the event horizon is a $(D-1)$-dimensional null hypersurface. In this study we will only consider $D = 4$. Then the event horizon surface is a three-dimensional null hypersurface (e.g. $r = 2m$ null surface in the Schwarzschild spacetime).

2.3 Trapped Surfaces

An event horizon is one of the defining features of a black hole. However it crucially depends on the structure of null infinity of the spacetime. Since the event horizon is teleological in nature, it is not the most convenient characterization of a black hole, especially when we aim to understand highly dynamical situations.

Gravity determines the causal structure of spacetime. It alters the path of light rays and the stronger the gravity the stronger the effect on the light. In the case of a black hole, sufficient mass is concentrated in a small enough region so as to not only deflect light, but literally drag it backwards. This is well explained by the concept of the *trapped surfaces*. Roger Penrose [42] defined a trapped surface as a closed compact spacelike two surface $\mathcal{S}$ such that the null expansions orthogonal to $\mathcal{S}$ are both negative. Here null expansions orthogonal to $\mathcal{S}$ means that expansions along each of the two future-pointing null directions ℓ^+ and ℓ^- that are normal to $\mathcal{S}$. From the definition of the expansion scalar for a surface, we can say that for a trapped surface,

$$\theta_{(\ell^+)} = q^{\alpha\beta}\nabla_\alpha \ell^+_\beta < 0 \qquad \text{and} \qquad \theta_{(\ell^-)} = q^{ab}\nabla_a \ell^-_b < 0, \tag{2.11}$$

where $q_{\alpha\beta}$ is the induced metric on $\mathcal{S}$. For convenience we cross-normalize, that is, $\ell^+ \cdot \ell^- = -1$ and assign one of these directions to be outward and other one is inward. Note that here we have assumed $\mathcal{S}$ to be orientable and the condition $\ell^+ \cdot \ell^- < 0$ comes from the fact that both null directions ℓ^+ and ℓ^- are future-pointing. To understand this, consider an embedded two sphere ($\mathbb{S}^2$) in Minkowski spacetime. Imagine, from the surface of this sphere, a pulse of light is emitted. In such a situation, light will move both outward from the surface, and also inward. The radius of the outward moving pulse increases, while that of the inward moving pulse decreases. This simple situation should be contrasted with what would happen for a trapped surface. Due to the presence of strong gravity in case of trapped surfaces, the expansion in both null directions are negative, that is, it will contract in both directions.

A *marginally outer trapped surface* (MOTS), is a closed spacelike two surface for which the expansion scalar vanishes in the outward null direction. To continue the analogy of the previous paragraph, for a MOTS the light moving in the outward direction instantaneously hovers there. The radius of the surface neither increases nor decreases. Note that unlike trapped surfaces, nothing is said about the expansion along the other null direction of a MOTS. A MOTS can be considered a limiting surface of the trapped surfaces in a three dimensional hypersurface of the spacetime. A simple example is a spatial slice of the $r = 2m$ event horizon in the Schwarzschild spacetime. More generally, two dimensional spacelike slice of horizons in stationary spacetimes (Kerr-Newman family) are also MOTS.

Another similar useful concept associated with trapped surfaces is *apparent horizon*. For a spacetime can be foliated by asymptotically flat spacelike three surfaces (Σ), a point in Σ is said to be trapped if it lies on some trapped two surface in Σ. An apparent horizon in Σ is is the boundary of the union of all of the trapped points in Σ [29]. Though it can be shown that apparent horizon is a MOTS with some certain smoothness assumptions, a MOTS in Σ may not be an apparent horizon.

2.4 Light Rays in Schwarzschild Geometry

The Schwarzschild metric in the standard Schwarzschild coordinate system (t,r,θ,ϕ) is,

$$\mathrm{d}s^2 = -\left(1 - \frac{2m}{r}\right)\mathrm{d}t^2 + \frac{\mathrm{d}r^2}{1 - \frac{2m}{r}} + r^2\mathrm{d}\theta^2 + r^2\sin^2\theta\,\mathrm{d}\phi^2\,. \tag{2.12}$$

Clearly, it has no dependence on time coordinate t or angular coordinate ϕ. This implies that vectors in ∂_t and ∂_ϕ are Killing vectors. In the standard Schwarzschild coordinate system, the components of the corresponding Killing vectors are

$$\eta^\alpha = (1, 0, 0, 0)\,, \tag{2.13}$$

$$\nu^\alpha = (0, 0, 0, 1)\,. \tag{2.14}$$

Each Killing vector implies a conserved quantity. If u^α is the four-velocity of photon, the conserved quantities for light rays will be $\eta \cdot u$ and $\nu \cdot u$.

Now, let λ be the affine parameter of null geodesics that describes the light rays. The tangent to the null geodesics is

$$u^\alpha \equiv \frac{\mathrm{d}x^\alpha}{\mathrm{d}\lambda} \equiv \dot{x^\alpha}\,. \tag{2.15}$$

Then the conserved quantities are

$$E = -\eta \cdot u = -g_{\alpha\beta}\eta^\alpha u^\beta = -g_{tt}\eta^t u^t = \left(1 - \frac{2m}{r}\right)\frac{\mathrm{d}t}{\mathrm{d}\lambda} = \left(1 - \frac{2m}{r}\right)\dot{t}\,, \tag{2.16}$$

$$L = \nu \cdot u = g_{\alpha\beta}\nu^\alpha u^\beta = g_{\phi\phi}\eta^\phi u^\phi = r^2 \sin^2\theta \frac{\mathrm{d}\phi}{\mathrm{d}\lambda} = r^2 \sin^2\theta \dot{\phi}\,, \tag{2.17}$$

where E is the energy and L is the angular momentum of photon. As a tangent of null geodesics, the norm of u vanishes

$$\begin{aligned} u \cdot u &= g_{\alpha\beta}u^\alpha u^\beta = 0 \\ \Longrightarrow -\left(1 - \frac{2m}{r}\right)\dot{t}^2 &+ \frac{\dot{r}^2}{\left(1 - \frac{2m}{r}\right)} + r^2\dot{\theta}^2 + r^2\sin^2\theta\dot{\phi}^2 = 0\,. \end{aligned} \tag{2.18}$$

Putting the conserved quantities E, L together with equation (2.18), we get,

$$\dot{r}^2 = E^2 - (1 - \frac{2m}{r})(r^2\dot{\theta}^2 + \frac{L^2}{r^2\sin^2\theta})\,. \tag{2.19}$$

As Schwarzschild spacetime has spherical symmetry, we can focus on equatorial plane ($\theta = \pi/2$) without losing any generality. The conserved quantity equations (2.16) and (2.17) along with the above equation (2.19) in the equatorial plane take the form,

$$\dot{t} = \frac{E}{\left(1 - \frac{2m}{r}\right)} \,, \tag{2.20}$$

$$\dot{\phi} = \frac{L}{r^2} \,, \tag{2.21}$$

$$\dot{r} = \sqrt{E^2 - \left(1 - \frac{2m}{r}\right) \frac{L^2}{r^2}} \,. \tag{2.22}$$

These above three equations are used to trace light rays in the Schwarzschild spacetime.

Chapter 3

Event Horizon During Extreme Mass Ratio Limit Black Hole Mergers

Following the discovery of stellar black hole merger, humanity obtained a new way to understand the universe. For the first time, in 2015 September, a gravitational wave signal (GW150914) was detected by the Laser Interferometer Gravitational-Wave Observatory (LIGO) along with its European counterpart Virgo [22, 21]. The signal came from two black holes spiralling in to each other and merging. This is called black hole merger.

Black hole mergers can be described by Einstein's field equations in vacuum, $R_{\mu\nu} = 0$, which are non-linear second order partial differential equations. Due to their non-linear nature, the solution of the equations is non-trivial in the sense that these equations are not easily solvable and it is difficult to extract information from them.

However in some regimes, these equations significantly simplify. In this chapter, one such a case will be discussed in detail.

Consider a black hole merger where one of the two participant black holes is much larger than the other. That is, the mass ratio, $\frac{m}{M} \to 0$, where m and M are masses of small and large black hole, respectively. Such mergers are called *extreme mass ratio mergers* (EMR). These mergers can be viewed in two different ways. The first kind focuses on the large black hole and considers the small black hole as an infalling point particle. In other words, we fix the mass of large black hole, M whereas the mass of the small black hole $m \to 0$. This approach is certainly beneficial for getting information about gravitational wave that emits from the collision. Although the approach is not so useful for understanding events on the scale of m, this approach has been studied extensively for a number of reasons [36, 35, 54]. For example, recently Hussain and Booth [32] used this EMR merger as a point particle plunging into Schwarzschild black hole to investigate the evolution of perturbed horizons using the Zerilli formalism [59]. A disadvantage of this approach is it misses out on information on the small black hole length scale which is crucial to get a full picture of horizon evolution.

An alternative picture which allows us to understand the physics on the scale of the small black hole, focuses on the small black hole [17]. This method of viewing the extreme mass ratio mergers keeping m fixed while the mass of large black hole (M) goes to infinity, so that the mass ratio again becomes zero, i.e.

$$\lim_{M \to \infty} \frac{m}{M} = 0\,. \tag{3.1}$$

If this approach is taken, the equivalence principle can be employed to simplify the problem greatly. According to the principle, no local experiment can distinguish free fall in an accelerated frame from uniform motion in an inertial frame provided that the acceleration is uniform. In the case of an extreme mass ratio merger, the movement of a small black hole towards the large black hole can be approximated as a free fall motion. For an observer in the rest frame of the small black hole, this free fall motion will be equivalent to no motion in an inertial frame (no gravity). So, in the rest frame of the small black hole one can ignore the curvature of the large black hole at a distance very much less than the size of large black hole ($\ll M$) as long as the small one is in motion. The implications of this are two-fold. First, in the case where the small black hole is non-rotating, the spacetime near the small black hole is approximated by the Schwarzschild space time. Secondly, it also makes the tidal force of the big black hole on the small black hole negligible. As a result there will be no tidal force distortion of the small black hole as it move towards the big one.

Though the effect of curvature of the large black hole is negligible in this extreme mass ratio limit, the horizon is still present and shields the events inside it from causally influencing the small black hole. As $M \gg m$, the large black hole horizon appears to be a null planar surface in the local frame of the small black hole. This planar horizon can be compared to a *Rindler Horizon*. Similar to the Rindler horizon, the horizon of the large black hole appears to be an infinite null plane if we focus on the small black hole length scale in this limit.

From the point of view of the small black hole, it will be reasonable to assume that a long time after the merger, the event horizon will settle down to be the event horizon of the large black hole, that is, a null plane. This suggests that the horizon of the merger can be found by tracing a family of null geodesics in Schwarzschild geometry that approach the null planar horizon asymptotically.

3.1 Null Geodesic Equations

Here we will use the geodesic equations for light rays that we derived at the end of the last chapter. The equations are,

$$\dot{t} = \frac{E}{\left(1 - \frac{2m}{r}\right)}\,, \tag{3.2}$$

$$\dot{\phi} = \frac{L}{r^2}\,, \tag{3.3}$$

$$\begin{aligned} \dot{r} &= \sqrt{E^2 - \left(1 - \frac{2m}{r}\right)\frac{L^2}{r^2}} \\ &= \frac{1}{r}\sqrt{E^2 r^2 - \left(1 - \frac{2m}{r}\right)L^2}\,. \end{aligned} \tag{3.4}$$

Without loss of generality, we take, $E = 1$, which makes the impact parameter, $q = \frac{L}{E} = L$. Then putting the values of E, L the above equations become:

$$\dot{t} = \frac{1}{\left(1 - \frac{2m}{r}\right)}\,, \tag{3.5}$$

$$\dot{\phi} = \frac{q}{r^2}\,, \tag{3.6}$$

$$\dot{r} = \frac{1}{r}\sqrt{r^2 - \left(1 - \frac{2m}{r}\right)q^2}\,. \tag{3.7}$$

These three equations (3.5), (3.6) and (3.7) are the ones we must solve to trace null geodesics in the Schwarzschild spacetime. For convenience, we will assume without loss of generality that the black holes will merge along the z-axis towards $\phi = \pi$ direction where $z = r\cos\phi$. In other words, merging will take place along a straight line towards the opposite direction of $\phi = 0$ with respect to the small black hole.

3.2 Simplification

In the equatorial plane, the space (t, r, ϕ) is three dimensional and the event horizon in this section is a one-parameter family of null geodesics (i.e. two dimensional surface). Note that like E and L, q is also a conserved quantity and unique to each null geodesics. Different values of q differentiate the geodesics from each other. This parameter q and the affine parameter λ along the geodesics are two variables of the two dimensional event horizon surface. To find the event horizon of the merger, one needs to solve the above mentioned three differential equations (3.5), (3.6) and (3.7) for three unknowns, $t_q(\lambda)$, $r_q(\lambda)$ and $\phi_q(\lambda)$. Here, subscript q denotes the concerned variable is calculated for a fixed value of q.

One way to do this is to integrate (3.7) to get $r_q(\lambda)$ and use it in (3.5) and in (3.6) to get $t_q(\lambda)$ and $\phi_q(\lambda)$. But the integration of (3.7) gives $\lambda_q(r)$ as a combination of complex elliptic integrals which are not easily invertible to find $r_q(\lambda)$. A more convenient way is to consider r as the non-affine parameter instead of λ. This choice is reasonable as the right-hand side of all the equations have r in them and it will reduce the number of equations and unknowns to two. Doing so gives

$$t_q(r) = \int \frac{\dot{t}}{\dot{r}}\mathrm{d}r = \int \frac{r^3\mathrm{d}r}{(r-2m)\sqrt{r(r^3 - q^2(r-2m))}} \tag{3.8}$$

and,

$$\phi_q(r) = \int -\frac{\dot{\phi}}{\dot{r}}\mathrm{d}r = \int \frac{q\mathrm{d}r}{\sqrt{r(r^3 - q^2(r-2m))}}\,. \tag{3.9}$$

Next we will consider the boundary conditions necessary for the integration of these equations.

3.3 Boundary Condition

The integration constant of the above integrals is fixed by the boundary condition that is the horizon surface becomes a null plane at infinity. We can break this into the following two conditions:

1. The null geodesics move in the same direction asymptotically. In other words, at infinity ($r \to \infty$), the angle ϕ has to be the same for all light rays, i.e. q independent.

2. Secondly, all the rays should reach future null infinity $\mathscr{I}^+$ at the same time.

Now, let us fix the integration constants using the above conditions. For ϕ_q, the asymptotic expansion of the integrand in (3.9) as $r \to \infty$ gives,

$$\left.\frac{\dot{\phi}}{\dot{r}}\right|_{r\to\infty} = -\frac{q}{r^2} + \mathcal{O}\left(\frac{1}{r^4}\right) . \tag{3.10}$$

So, asymptotically,

$$\left.\phi_q\right|_{r\to\infty} = \left[\int \frac{\dot{\phi}}{\dot{r}} \mathrm{d}r\right]_{r\to\infty} = \alpha + \frac{q}{r} + \mathcal{O}\left(\frac{1}{r^3}\right) . \tag{3.11}$$

Here, α is the integration constant.

From equation (3.11), it is clear that at infinity, except the first term, all the other terms vanish on the right-hand side. So α is the asymptotic angle of the null geodesics. According to the first boundary condition, the angle ϕ is required to be same for any value of q. This implies α has to be q independent. Therefore α must be constant with respect to q. Now, if we take α as zero, asymptotically the light rays will reach a null planar surface which is oriented perpendicular to the z-axis. This will simplify our calculation. Without loss of generality, we take,

$$\alpha = 0. \tag{3.12}$$

Let us introduce a new set of coordinates, $(t = t,\ x = r\sin\phi,\ z = r\cos\phi)$. Note that, this new z-coordinate is consistent with earlier definition of z. Assuming that the boundary conditions are satisfied, the horizon surface indeed becomes a null plane that is z-axis perpendicular at infinity. This can also be seen by doing a simple calculation involving new coordinates, x and z. At $r \to \infty$,

$$\begin{aligned} z_q &= r\cos(\phi_q) \\ &= r\cos\left(\alpha + \frac{q}{r} + \mathcal{O}(r^{-3})\right) \\ &= r + \mathcal{O}(r^{-1})\,. \end{aligned} \tag{3.13}$$

Here we used (3.9) and the fact that $\cos(\phi) \approx 1$ when $\phi \ll 1$ to arrive at this result. Similarly, asymptotically,

$$\begin{aligned} x_q &= r\sin(\phi_q) \\ &= r\sin\left(\alpha + \frac{q}{r} + \mathcal{O}(r^{-3})\right) \\ &= r\sin\left(\frac{q}{r}\right) + \mathcal{O}(r^{-3}) \\ &= q + \mathcal{O}(r^{-3})\,. \end{aligned} \tag{3.14}$$

This follows from $\sin\phi \approx \phi$ for $\phi \ll 1$.

The above result shows that the null geodesics are moving along the z-axis as $\dot{x} \to 0$ asymptotically. It also gives the impact parameter q a physical meaning. It is the asymptotic distance of the corresponding null geodesic from z-axis.

Coming back to the integration constant for t_q, an asymptotic expansion of the integrand of (3.8) at $r \to \infty$ gives us,

$$\left.\frac{\dot{t}}{\dot{r}}\right|_{r\to\infty} = 1 + \frac{2m}{r} + \mathcal{O}(r^{-2})\,. \tag{3.15}$$

So asymptotically,

$$t_q\big|_{r\to\infty} = \left[\int \mathrm{d}r \frac{\dot{t}}{\dot{r}}\right]_{r\to\infty} = r + 2m\ln\left(\frac{r}{2m}\right) + \beta + \mathcal{O}(r^{-1})\,. \tag{3.16}$$

The integration constant β can be fixed so that all the light rays reach $\mathscr{I}^+$ at the same time. For this to be true, t_q is required to be independent of q asymptotically. Note that the first two terms on the right-hand side of equation (3.16) do not depend on q. To ensure asymptotic t_q is independent of q, the integration constant β needs to be q-independent. For convenience, we choose,

$$\beta = 0. \tag{3.17}$$

After fixing the integration constants α and β, we found our boundary conditions to be,

$$\phi_q|_{r\to\infty} = \mathcal{O}(r^{-1})\,, \tag{3.18}$$

and

$$t_q|_{r\to\infty} = r + 2m\ln\left(\frac{r}{2m}\right) + \mathcal{O}(r^{-1}). \tag{3.19}$$

3.4 Numerical Solution

Emparan and Martínez [17] have shown that (3.8) and (3.9) can be solved exactly. However, the solutions are very complex expressions involving incomplete elliptic integrals of the first, second and third kinds, which are not very insightful. Of course, the figures produced from these expressions are certainly meaningful. Similar results can be achieved by solving the equations numerically.

In this section we will discuss the numerical method and the results obtained from this numerical analysis. The tool we used for integrating (3.8) and (3.9) is *Maple 2018.2*. We integrate the equations from $r = \infty$ to $r = r'$ to get the numerical values of $t(r')$ and $\phi(r')$ to produce the figure 3.1. The boundary conditions used here are (3.18) and (3.19) at $r = \infty$ and starting the integration at infinity automatically implements these conditions. However, a subtlety in this calculation is that (3.19) has terms that diverge like r and $\ln r$ near $r = \infty$. To fix this we first adjusted the integrand in (3.8) by subtracting $\dot{t}/\dot{r}|_{r\to\infty}$ in (3.15) (the integrand in (3.8) at infinity) from it and then added $t_q|_{r\to\infty}$ from (3.19) after the integration.

$$\begin{aligned} t_q(r') &= t_q|_{r'\to\infty} + \int_{\infty}^{r'} \left(\frac{\dot{t}}{\dot{r}} - \left.\frac{\dot{t}}{\dot{r}}\right|_{r\to\infty} \right) \mathrm{d}r \\ &= r' + 2m \ln\left(\frac{r'}{2m}\right) + \int_{\infty}^{r'} \left(\frac{r^3}{(r-2m)\sqrt{r(r^3 - q^2(r-2m))}} - 1 - \frac{2m}{r} \right) \mathrm{d}r \,. \end{aligned} \tag{3.20}$$

Figure 3.1 shows time evolution of spacelike slice of the event horizon generated by the light rays from future infinity with two different views at $\theta = \pi/2$. As we mentioned before, each light ray has a distinct value of q. In full three dimensions (consider full range of θ), the event horizon generators lie on a $\mathbb{S}^1$ of radius q at future infinity. At early times, the event horizon of the merger consists of three parts: the event horizon of small black hole, the event horizon of large black hole and a line connecting them, where at each point, two light rays from $\mathscr{I}^+$ intersect each other. These points are known as *caustics*. There are two special q-values where

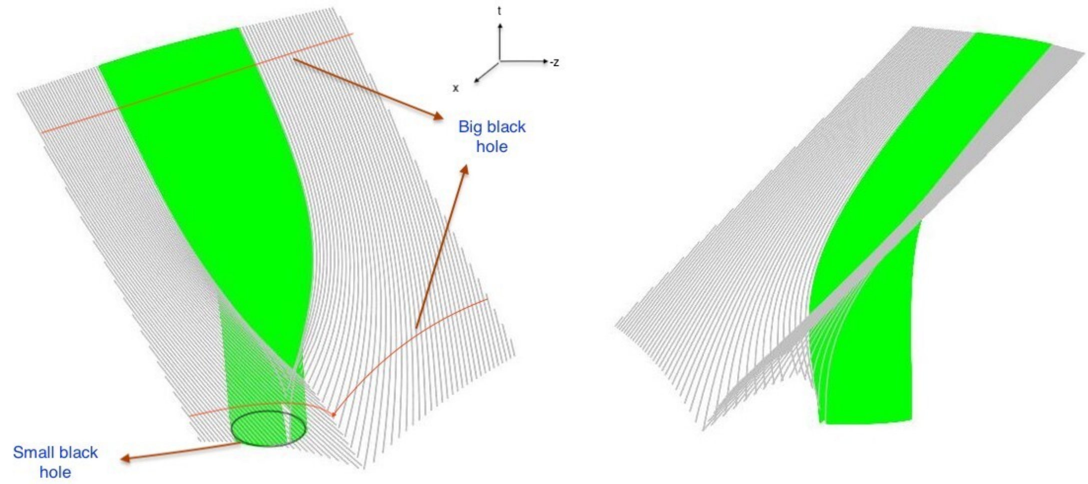

Figure 3.1: Two different views of the event horizon of the four-dimensional merger, in the rest frame of the small black hole. In both of them, the crease in the lower portion consists of caustic points where light rays meet.

there is a change in behaviour of the null generators: q_c and q^*. All generators with $-q_c < q < q_c$ are called *non-caustic generators.* They do not end up in a caustic point. These light rays can be thought of as those that just barely escaped the small black hole to make it to infinity. The generators with critical value q_c starts at the Schwarzschild horizon at $\phi = \pi$. For $q > |q_c|$, the generators focus at caustics at finite times to become a part of the event horizon. These generators are called *caustic generators.* These generators can be further divided into two different kinds based on the angle at which they intersects the line of caustics. For $|q_c| < |q| < |q^*|$, the the light rays meet while directed toward the small black hole, while for $|q| > q^*$, the light rays are directed away from the small black hole when they meet. The generator with critical value q^* intersects the line of caustics perpendicularly.

The importance of the work done by Emparan and Martínez lies in the fact the complex problem of black hole mergers involving non-trivial field equations that could have otherwise required heavy resources (e.g. supercomputers), is reduced to a problem involving null geodesics and Schwarzschild geometry. The conceptual ingredient used for this is the equivalence principle which is the founding principle of general relativity itself. In the next chapter, we will discuss marginally outer trapped surfaces (MOTS) as an alternative to event horizons and present our effort to explain the time evolution of MOTS during extreme mass ratio mergers.

Chapter 4

MOTOS in Schwarzschild Geometry with EMR Setup

The evolution of event horizons during a black hole merger is a complex phenomenon in General relativity. The work of Emparan and Martínez that we explored in the previous chapter provides a simple way to understand aspects of this complex phenomenon. However, as we mentioned in the first chapter, the definition of event horizon depends on the global causal structure of the spacetime, rather than the local properties of spacetime. Because of this, the event horizon is of limited value to describe dynamical phenomena like black hole mergers.

As we discussed in the introduction, the concept of a trapped surface is closely connected to the properties of black holes. Marginally outer trapped surface (MOTS) can be treated as the boundary of all the trapped surface for a spacelike slice of spacetime. It is a quasi-local concept that can be used as a proxy for event horizon to understand black hole mergers.

On the other hand, during extreme mass ratio mergers the spacetime close to a small black hole can also be approximated by the Schwarzschild spacetime and the large black hole horizon as an ‘open’ null plane. It is expected that the MOTS during extreme mass ratio mergers, close to small black hole can also approximated by spacelike open surfaces with vanishing null expansion in the Schwarzschild spacetime. The purpose of our work is to understand the possible behaviours of MOTS during the EMR set up described by Emparan and Martínez. We found interesting results pertaining to open and closed axisymmetric marginally trapped surfaces in the Schwarzschild geometry. In this chapter we will discuss these results and try to interpret them in a meaningful way.

4.1 MOTOS and Schwarzschild Geometry

In this analysis we are interested in MOTS: two dimensional spacelike surfaces in the four dimensional Schwarzschild geometry. The normal space to each point of a spacelike two dimensional surface is timelike and two dimensional in a four dimensional spacetime. Generally, for any spanning pair of vectors of a two dimensional timelike space, if they are chosen to be orthogonal, then one of them has to be timelike and other one spacelike. However, if we relax the orthogonality criteria, a timelike two dimensional surface can be spanned by two null vectors.

A four dimensional Schwarzschild spacetime can be decomposed into three dimensional hypersurfaces. These hypersurfaces are specified as the level sets of a real-valued smooth function. Here for our purpose, we will consider constant time hypersurfaces Σ, the interpretation of which depends on the coordinate system of the spacetime. This induces a metric on the hypersurface, h_{ij} and a timelike normal to it. These hypersurfaces are spacelike and any two dimensional surfaces in them will also be spacelike as a spacelike three dimensional surface does not contain any timelike or null component. For convenience, we only consider here axisymmetric two dimensional surfaces, $\mathcal{S}$. Within the hypersurface Σ, $\mathcal{S}$ has a spacelike normal. Then the normal space of $\mathcal{S}$ embedded in a four dimensional Schwarzschild spacetime is timelike, which is spanned by the above mentioned timelike normal and spacelike normal orthogonally. It can also be spanned by two non-orthogonal null vectors, ℓ^+ and ℓ^-. It is possible to construct these two null directions from the spacelike normal and timelike normal. For convenience, we choose to cross-normalize such that,

$$\ell^+ \cdot \ell^- = -1\,. \tag{4.1}$$

The expansions associated to these normals are

$$\theta^+ = q^{\alpha\beta}\nabla_\alpha \ell^+_\beta \qquad \text{and} \qquad \theta^- = q^{\alpha\beta}\nabla_\alpha \ell^-_\beta\,, \tag{4.2}$$

where

$$q_{\alpha\beta} = e^A_\alpha e^B_\beta q_{AB} = g_{\alpha\beta} + \ell^+_\alpha \ell^-_\beta + \ell^-_\alpha \ell^+_\beta\,, \tag{4.3}$$

where q_{AB} is the induced metric on $\mathcal{S}$ and $g_{\alpha\beta}$ is the spacetime metric. In these expressions Greek letters and capital latin letters are respectively spacetime and surface indices and e^A_α is the pullback/push forward operator between the spaces.

Now, given a parameterization, the null expansion of a two dimensional surface is determined by a second order differential operator. So, the surface with vanishing null expansion is required to satisfy a second order differential equation. Equally, given a point in a spacetime and a tangent plane at that point, the differential equation can be solved with constraints in order to get the surfaces with vanishing null expansion. This tactic is employed in this project to find spacelike two dimensional surfaces with vanishing null expansion.

We define a *marginally outer trapped open surface* (MOTOS) to be an open spacelike two dimensional surface with (at least) one normal direction of vanishing null expansion. We will refer to that direction as outward. In the upcoming sections, we will study axisymmetric MOTOS in three different coordinate systems with stationary or non-stationary slices.

4.2 MOTOS in Schwarzschild Coordinates

First we will work with the standard Schwarzschild coordinates which are singular at $r = 2m$. The metric expressed in this coordinate system is

$$\mathrm{d}s^2 = -\left(1 - \frac{2m}{r}\right)\mathrm{d}t^2 + \frac{\mathrm{d}r^2}{1 - \frac{2m}{r}} + r^2\mathrm{d}\theta^2 + r^2\sin^2\theta\mathrm{d}\phi^2\,. \tag{4.4}$$

4.2.1 Foliation of Spacetime and 2D Surfaces

Starting with a spacelike hypersurface of constant t, Σ_t in the Schwarzschild standard coordinates,

$$t_\Sigma = \text{constant}, \tag{4.5}$$

with unit timelike normal

$$u = u_\alpha \mathrm{d}x^\alpha = -\sqrt{1 - \frac{2m}{r}}\mathrm{d}t\,. \tag{4.6}$$

The hypersurface is extrinsically flat as the extrinsic curvature

$$\begin{aligned} K_{\alpha\beta} &= \nabla_\alpha u_\beta \\ &= \frac{\partial u_\beta}{\partial x^\alpha} - \Gamma^\gamma_{\alpha\beta} u_\gamma = 0. \end{aligned} \tag{4.7}$$

where ∇_α denotes covariant derivative and $\Gamma^\gamma_{\alpha\beta}$ denotes the Christoffel symbol for the full metric (4.4). The induced metric on the hypersurface is

$$h_{ij}\mathrm{d}x^i\mathrm{d}x^j = \frac{\mathrm{d}r^2}{1-\frac{2m}{r}} + r^2\mathrm{d}\theta^2 + r^2\sin^2\theta\mathrm{d}\phi^2, \tag{4.8}$$

where $x^i = (r, \theta, \phi)$ denotes the coordinates of hypersurface Σ.

A general axisymmetric two dimensional surface $\mathcal{S}$ in Σ_t, cannot be covered by a single coordinate patch. For a surface that is rotationally symmetric about the ϕ axis, a convenient parameterization is

$$r = R(\lambda), \qquad \theta = \Theta(\lambda) \qquad \text{and} \qquad \phi = \phi, \tag{4.9}$$

for R and Θ are some functions of λ. The induced metric on $\mathcal{S}$ can easily be found by applying (4.9) in (4.8) as:

$$q_{AB}\mathrm{d}x^A\mathrm{d}x^B = \left(\frac{\dot{R}^2}{1-\frac{2m}{R}} + R^2\dot{\Theta}^2\right)\mathrm{d}\lambda^2 + R^2\sin^2\Theta\mathrm{d}\phi^2, \tag{4.10}$$

where the dot denotes the derivative with respect to λ. Here, $x^A = (\lambda, \phi)$ is a point in the coordinate patch that covers only $\mathcal{S}$. The tangents are

$$e_\lambda = \frac{\mathrm{d}}{\mathrm{d}\lambda} = \dot{R}\frac{\partial}{\partial r} + \dot{\Theta}\frac{\partial}{\partial\theta}, \tag{4.11}$$

and

$$e_\phi = \frac{\mathrm{d}}{\mathrm{d}\phi}. \tag{4.12}$$

The unit spacelike normal to the two dimensional surface $\mathcal{S}$ is,

$$n = n_i \mathrm{d}x^i = A\left(-\dot{\Theta}\frac{\partial}{\partial r} + \dot{R}\frac{\partial}{\partial \theta}\right), \tag{4.13}$$

where

$$A = \left(\frac{\dot{R}^2}{R^2} + \frac{\dot{\Theta}^2}{1 - \frac{2m}{R}}\right)^{-1}. \tag{4.14}$$

4.2.2 Null Expansions

At each point, the normal space to the two dimensional surface $\mathcal{S}$ is spanned by two null vectors that can be constructed from the timelike and spacelike normals defined above.

$$\ell^+ = u + n, \qquad \text{and} \qquad \ell^- = \frac{1}{2}(u - n). \tag{4.15}$$

So, the null expansions are

- along ℓ^+ direction,

$$\theta^+ = q^{\alpha\beta}\nabla_\alpha \ell^+_\beta\,, \tag{4.16}$$

- along ℓ^- direction,

$$\theta^- = q^{\alpha\beta}\nabla_\alpha \ell^-_\beta\,, \tag{4.17}$$

where

$$q^{\alpha\beta} = q^{ij} e^\alpha_i e^\beta_j = (q^{AB} e^i_A e^j_B) e^\alpha_i e^\beta_j\,. \tag{4.18}$$

In the above, e^i_A are the push forward/pullback operator between the hypersurface Σ_t and the two dimensional surface $\mathcal{S}$ and e^α_i are the push forward/pullback operator between the Schwarzschild spacetime and the hypersurface Σ_t. From the relationship between the spacetime coordinates (x^α) and the hypersurface coordinates (x^i)

$$r_\Sigma = r, \qquad \theta_\Sigma = \theta, \qquad \text{and} \qquad \phi_\Sigma = \phi\,. \tag{4.19}$$

We can easily calculate the corresponding push forward/pullback operator,

$$e_i^\alpha = \frac{\partial x^\alpha}{\partial x^i} = \begin{pmatrix} 0 & 0 & 0 \\ 1 & 0 & 0 \\ 0 & 1 & 0 \\ 0 & 0 & 1 \end{pmatrix}. \tag{4.20}$$

Similarly, the push forward/pullback operator between hypersurface coordinates (x^i) and surface coordinates (x^A) can be derived from (4.9),

$$e_A^i = \frac{\partial x^i}{\partial x^A} = \begin{pmatrix} \dot{R} & 0 \\ \dot{\Theta} & 0 \\ 0 & 1 \end{pmatrix}. \tag{4.21}$$

Putting all this together, we find for the expansion in the direction of ℓ^+:

$$\begin{aligned} \theta^+ &= q^{\alpha\beta}\nabla_\alpha(u_\beta + n_\beta) = q^{\alpha\beta}K_{\alpha\beta} + q^{\alpha\beta}\nabla_\alpha n_\beta \\ &= q^{\alpha\beta}\nabla_\alpha n_\beta \\ &= q^{\alpha\beta}k_{\alpha\beta} = k\,, \end{aligned} \tag{4.22}$$

while for the expansion in the direction of ℓ^- we find

$$\begin{aligned} \theta^- &= \frac{1}{2}q^{\alpha\beta}\nabla_\alpha(u_\beta - n_\beta) = \frac{1}{2}q^{\alpha\beta}K_{\alpha\beta} - \frac{1}{2}q^{\alpha\beta}\nabla_\alpha n_\beta \\ &= -\frac{1}{2}q^{\alpha\beta}\nabla_\alpha n_\beta \\ &= -\frac{1}{2}q^{\alpha\beta}k_{\alpha\beta} = -\frac{1}{2}k\,. \end{aligned} \tag{4.23}$$

Here, in both the cases, we used (4.15) first and then the fact that the constant time hypersurface (Σ_t) is extrinsically flat, (4.7) is used. In the above, $k_{\alpha\beta} = \nabla_\alpha n_\beta$ is the extrinsic curvature of $\mathcal{S}$, the two dimensional surface imbedded in the hypersurface and $k = q^{\alpha\beta} k_{\alpha\beta}$ is the trace of extrinsic curvature of $\mathcal{S}$. If the trace of extrinsic curvature, k vanishes, the $\mathcal{S}$ becomes a minimal surface.

4.2.3 Equation of MOT(O)S

From (4.22) and (4.23), it can be easily seen that both the null expansions along ℓ^+ and ℓ^- cannot vanish independently. For vanishing k, the expansions $\theta^\pm$ vanish simultaneously. So, MOT(O)S are minimal surfaces in constant time hypersurfaces Σ in Schwarzschild coordinate system. Explicitly, the trace of the extrinsic curvature reads

$$\begin{aligned}
k &= q^{\alpha\beta}\nabla_\alpha n_\beta \\
&= q^{ij}\nabla_i n_j \\
&= A(q^{\lambda\lambda}(e^i_\lambda \partial_\lambda n_i - e^i_\lambda e^j_\lambda \Gamma^p_{ij} n_p) - q^{\phi\phi}(\Gamma^p_{\phi\phi} n_p)) \\
&= \frac{A}{R^2}\left(\frac{R(R-2m)(\dot{R}\ddot{\Theta} - \ddot{R}\dot{\Theta}) + 2\dot{\Theta}(2R(R-2m)^2\dot{\Theta}^2 + (3R-5m)\dot{R}^2)}{\dot{R}^2 + R(R-2m)\dot{\Theta}^2} - \dot{R}\cot\Theta\right),
\end{aligned} \tag{4.24}$$

where A was defined in equation (4.14). So for $\mathcal{S}$ to be a MOT(O)S, it needs to satisfy the following equation,

$$\frac{R(R-2m)(\dot{R}\ddot{\Theta} - \ddot{R}\dot{\Theta}) + 2\dot{\Theta}(2R(R-2m)^2\dot{\Theta}^2 + (3R-5m)\dot{R}^2)}{\dot{R}^2 + R(R-2m)\dot{\Theta}^2} - \dot{R}\cot\Theta = 0\,. \tag{4.25}$$

Here we have a single equation, written in terms of two unknown functions. The reason why this is consistent is because the parameterization is arbitrary: the actual surface does not depend on the particular choice of λ. For this reason, we are free to pick a parameterization that is convenient. As we will see, two such parameterizations are $\lambda = r$ or $\lambda = \theta$. The choice $\lambda = r$ gives,

$$
\begin{aligned}
&\Theta = \Theta(r)\,, \\
&\Theta_\lambda = \Theta_r\,, \\
&\Theta_{\lambda\lambda} = \Theta_{rr}\,, \\
&R_\lambda = R_r = 1 \text{ and} \\
&R_{\lambda\lambda} = R_{rr} = 0
\end{aligned}
$$

where subscript r denotes derivation with respect to r. Then, (4.25) will become

$$\Theta_{rr} - \left(\frac{1}{r(r-2m)} + \Theta_r^2\right)\cot\Theta + \Theta_r\left(2(r-2m)\Theta_r^2 + \frac{3r-5m}{r(r-2m)}\right) = 0\,. \tag{4.26}$$

For the other parameterization choice, that is for $\lambda = \theta$, we have

$$
\begin{aligned}
&R = R(\theta)\,, \\
&R_\lambda = R_\theta\,, \\
&R_{\lambda\lambda} = R_{\theta\theta}\,, \\
&\Theta_\lambda = \Theta_\theta = 1 \text{ and} \\
&\Theta_{\lambda\lambda} = \Theta_{\theta\theta} = 0
\end{aligned}
\tag{4.27}
$$

where subscript θ denotes derivation with respect to θ. Incorporating the above results in (4.25), we get,

$$R_{\theta\theta} + R_\theta \left(\frac{R_\theta^2}{R-2m} + 1 \right) \cot\theta - 2(R-2m) + \frac{5m-3R}{2R(R-2m)} = 0\,. \tag{4.28}$$

To get a continuous minimal surface requires both versions, (4.26) and (4.28) of the MOTS equations. Suppose we start out with (4.26), at some point if there is a local extremum in r, then

$$\frac{\mathrm{d}\Theta}{\mathrm{d}r} \to \infty\,.$$

Similarly for (4.28), if there is an extremum in θ, $\mathrm{d}R/\mathrm{d}\theta$ diverges. This can only avoided when one of these functions is monotonic, only then can the minimal surface be covered by a single patch. As we will see later, this is the reason that we need both the patches (θ, ϕ) and (r, ϕ) to cover a complete minimal surface.

4.2.4 Analytical Results

Here we explore the analytical aspects of the problem in order to build some understanding before solving it numerically.

4.2.4.1 Minkowski Limit $m = 0$

For $m = 0$, the problem reduces to finding rotationally symmetric minimal surfaces in Euclidean $\mathbb{R}^3$ space. A surface is minimal if its two principal curvatures are equal in magnitude but opposite in orientation. The trivial case is a $z =$ constant plane where $z = r\cos\theta$. For the $z =$ constant plane both principal curvatures vanish. An interesting non-trivial case is a catenoid (see figure 4.1) for which both the principal curvatures are equal in magnitude but opposite in orientation. The curvature associated with the rotational symmetry is oriented inwards towards the z-axis and so the

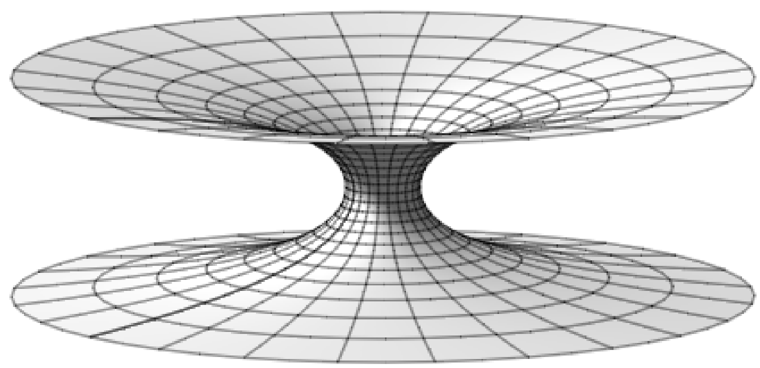

Figure 4.1: A catenoid in Euclidean $\mathbb{R}^3$

other must be outwards. These opposite orientations give catenoids their characteristic hyperbolic shape as seen in figure 4.2. In cylindrical coordinates (ρ,z,ϕ) where

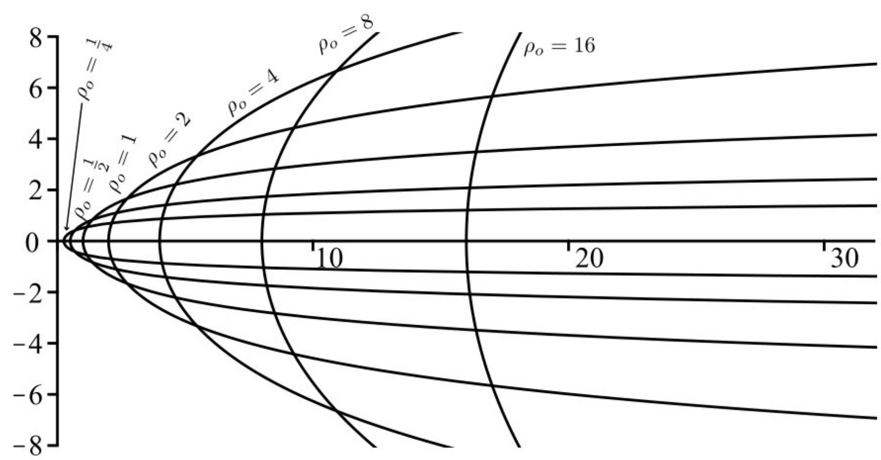

Figure 4.2: Cross-sections of minimal surfaces with $z_o = 0$ for Euclidean $\mathbb{R}^3$. Note that as $\rho_o \to 0$ the catenoid reduces to the $z = 0$ plane. For $z_o \neq 0$ the surfaces are appropriately shifted up or down in the z direction.

$\rho = r\sin\theta$ and $z = r\cos\theta$, a catenoid can be parameterized as

$$\rho = \rho_o \cosh\left(\frac{z - z_o}{\rho_o}\right) , \tag{4.29}$$

for $-\infty < z < \infty$ and $-\pi < \phi < \pi$. (ρ_o, ϕ, z_o) is the circle of closest approach to the z-axis. Figure 4.2 shows $z_o = 0$ catenoids in ρz-plane. Note the sharper curvature for those approaching closer to the z-axis. Converting to spherical coordinates with parameter $\lambda = z$ these become,

$$R(z) = \sqrt{\rho^2 + z^2} = \rho_o\sqrt{\cosh^2\left(\frac{z - z_o}{\rho_o}\right) + \left(\frac{z}{\rho_o}\right)} , \tag{4.30}$$

$$\Theta(z) = \tan^{-1}\left(\frac{\rho_o}{z}\cosh\left(\frac{z - z_o}{\rho_o}\right)\right) . \tag{4.31}$$

where $r = R(z)$, $\theta = \Theta(z)$. One can confirm this is a solution by directly substituting it in (4.25).

Let us now consider the case where minimal surfaces intersect the rotational symmetry axis (like Euclidean planes). The first two possibilities can be studied perturbatively.

4.2.4.2 Intersecting the Axis of Rotational Symmetry

To understand the behaviour of minimal surfaces that cross the z-axis where $\theta = 0$, we expand,

$$R(\theta) = \sum_{n=0}^{\infty} R_n \theta^n . \tag{4.32}$$

We incorporate the above ansatz in (4.28) and solve it order-by-order. Then the equation associated with the leading order term turns out to be

$$\frac{R_1(R_1^2 + R_0(R_0 - 2m))}{R_0(R_0 - 2m)\theta} = 0 . \tag{4.33}$$

For $R_0 > 2m$, the expression in brackets in the numerator is always positive. This means that the only possibility is $R_1 = 0$ in the limit $\theta \to 0$. The higher-order terms can then be obtained iteratively in terms of R_0. The first few of these terms read:

$$R = R_0 + \frac{R_0 - 2m}{2}\theta^2 + \frac{(10R_0 - 9m)(R_0 - 2m)}{48R_0}\theta^4 + \mathcal{O}(\theta^6). \tag{4.34}$$

In particular note that odd order coefficients R_1, R_3 etc. vanish. With $R_1 = 0$ any minimal surface that intersects the z-axis must do so at a right angle. Also the various terms all vanish if $R_0 = 2m$. This property extends to all orders in the perturbative expansion, and the reason is that the horizon itself is a minimal surface.

4.2.5 Numerical Results

Keeping the possible behaviours determined by the analytical insights from the last subsection 4.2.4, we will now solve the full minimal surface equations, (4.26) and (4.28). Here we will explore two cases: the first is when minimal surfaces intersect z-axis and the second when they intersect the horizon.

The minimal surface equations can be integrated numerically to find axisymmetric MOTOS. To circumvent the divergence problem associated with using the coordinate parameterization mentioned in subsection 4.2.3, we need both of the equations. The main idea is to switch between equations whenever we encounter a divergence problem. We start with an initial value (r_o, θ_o). As it is a second order equation, the initial value of first order derivative, $\mathrm{d}R/\mathrm{d}\theta|_{\theta_o}$ is also required. Now using these initial data, we integrate (4.28) as long as possible until we hit a singularity point. At that point we step back from the singular point to a point in the close neighbourhood $(r_1,\, \theta_1)$ and calculate $\mathrm{d}R/\mathrm{d}\theta|_{\theta_1}$. Now we will switch to (4.26). We can then use $(r_1,\, \theta_1)$ and

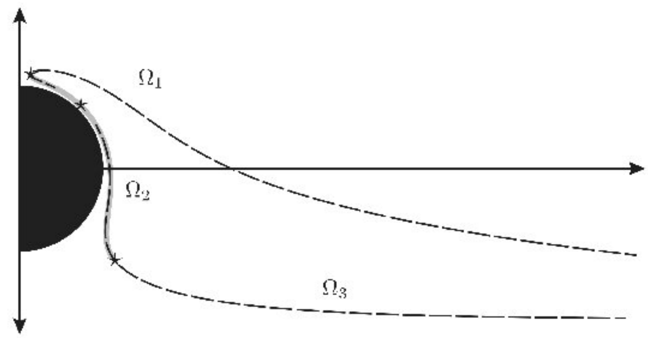

Figure 4.3: A minimal surface that comes close to $r = 2m$. The dashed segments are parameterized by functions $\Theta_1(r)$ and $\Theta_3(r)$ while the thick grey segment is parameterized by a function $R_2(\theta)$. At the starred endpoints of Ω_2, $\mathrm{d}R/\mathrm{d}\theta \to \infty$ (these are local extrema in θ). In the interior of Ω_2 a star also marks the point where $\mathrm{d}R/\mathrm{d}\theta = 0$ and so $\mathrm{d}\Theta/\mathrm{d}r \to \infty$. Both the patches together define the full surface.

$\mathrm{d}\Theta/\mathrm{d}r|_{r_1} = (\mathrm{d}R/\mathrm{d}\theta|_{\theta_1})^{-1}$ as initial data in (4.26). Again this is integrated until a singularity is encountered at which point we again step back from the singularity to a close point (r_2, θ_2) and calculate $\mathrm{d}\Theta/\mathrm{d}r|_{r_2}$. Then start again with (4.26) with initial data (r_2, θ_2) and $\mathrm{d}R/\mathrm{d}\theta|_{\theta_2} = (\mathrm{d}\Theta/\mathrm{d}r|_{r_2})^{-1}$. This is repeated until we exhaust our domain of interest.

Surfaces intersecting the z-axis are shown in figure 4.4. In accord with the series expansion (in subsection 4.2.4.2) these all intersect the axis at a right angle but intersect z-axis at different points. That is the R_0 value is different for different surfaces. These surfaces don't necessarily maintain their original ordering along the z-axis. For example, the surface starting from $z = 4$ intersects those starting close to the horizon. The surfaces originating from close to $r = 2m$ wrap around the black

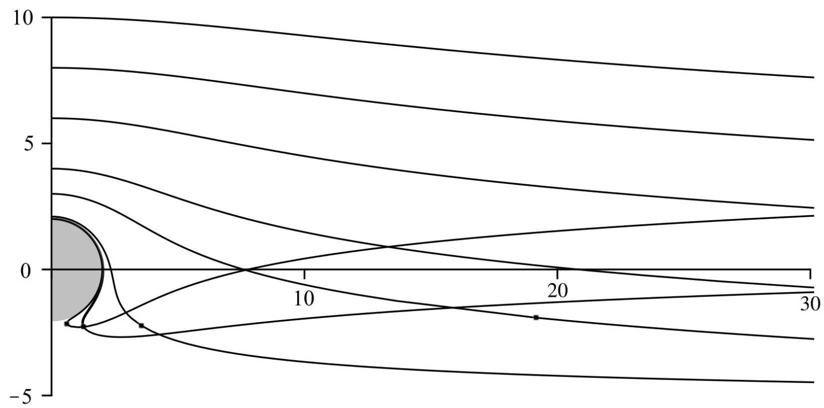

Figure 4.4: Minimal surfaces (MOTOS) intersecting the z-axis in Schwarzschild standard coordinate system. These were all integrated from the z-axis using the $R(\theta)$ equation (4.28). The dots indicate locations where we switched to the $\Theta(r)$ equation (4.26). There is a reflective symmetry for surfaces starting from negative z values.

hole before turning to head out to infinity. The closer to $2m$ that they start, the tighter they wrap and the further they reach before turning around. This behaviour also can be seen in figure 4.5, which shows surfaces that intersect the horizon. These

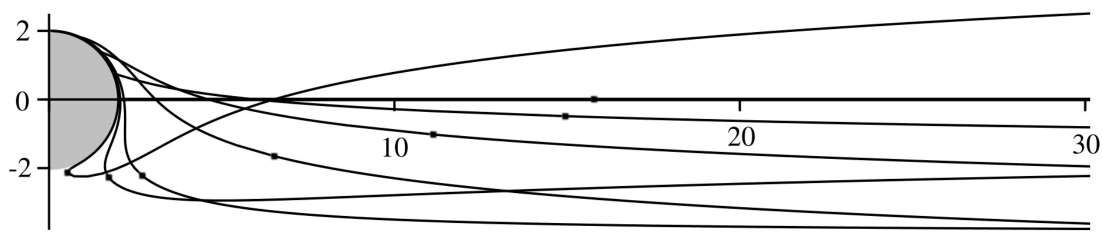

Figure 4.5: Minimal surfaces (MOTOS) that intersect the horizon in Schwarzschild standard coordinate system. These were all integrated from the horizon using the $R(\theta)$ equation (4.28). The dots indicate locations where we switched to the $\Theta(r)$ equation (4.26). There is a planar minimal surface running along the x-axis. There is a reflective symmetry for surfaces starting from negative z values.

were all integrated from the horizon using the $R(\theta)$ equation (4.28). The dots indicate locations where we switched to the $\Theta(r)$ equation (4.26). There is a planar minimal surface running along the x-axis in figure 4.5. There is a reflective symmetry for surfaces starting from negative z values.

4.3 MOTOS in Isotropic Cylindrical Coordinates

Next we choose to work in the isotropic cylindrical coordinates. In this coordinate system, constant time hypersurfaces are spacelike like the Schwarzschild standard coordinates. So, any two-surface contained within the spacelike hypersurface will necessarily be spacelike. The advantage of working in this coordinate system over the previous one is that the constant time slices are conformally flat (Euclidean $\mathbb{R}^3$ with a factor). The calculations regarding the two dimensional surfaces within the hypersurfaces can be expressed in coordinates similar to cartesian coordinates.

4.3.1 Metric

Let us introduce a new coordinate ϱ and a new function $\Delta(\varrho)$ such that the Schwarzschild metric (4.4) takes the form,

$$\mathrm{d}s^2 = -\left(1 - \frac{2m}{r}\right)\mathrm{d}t^2 + \Delta^2(\varrho)(\mathrm{d}\varrho^2 + \varrho^2\mathrm{d}\theta^2 + \varrho^2\sin\theta^2\mathrm{d}\phi^2)\,. \tag{4.35}$$

If we compare (4.35) with (4.4), then the following conditions must be satisfied,

$$r^2 = \Delta^2\varrho^2\,. \tag{4.36}$$

Furthermore,

$$\left(1 - \frac{2m}{r}\right)^{-1}\mathrm{d}r^2 = \Delta^2\mathrm{d}\varrho^2\,. \tag{4.37}$$

Putting the two conditions (4.36) and (4.37) together, we get

$$\frac{\mathrm{d}r}{\sqrt{r^2 - 2mr}} = \pm\frac{\mathrm{d}\varrho}{\varrho}\,. \tag{4.38}$$

If we choose + sign in (4.38) and integrate both side, we have

$$r = \varrho\left(1 + \frac{m}{2\varrho}\right)^2\,. \tag{4.39}$$

Using the above result in (4.36) gives

$$\Delta^2 = \left(1 + \frac{m}{2\varrho}\right)^4\,. \tag{4.40}$$

So, the final form of metric (4.35) in isotropic (spherical) coordinates,

$$\mathrm{d}s^2 = -\frac{\left(1-\frac{m}{2\varrho}\right)^2}{\left(1+\frac{m}{2\varrho}\right)^2}\mathrm{d}t^2 + \left(1+\frac{m}{2\varrho}\right)^4 (\mathrm{d}\varrho^2 + \varrho^2\mathrm{d}\theta^2 + \varrho^2 \sin\theta^2 \mathrm{d}\phi^2)\,. \tag{4.41}$$

The spatial part of the metric is the Euclidean metric in spherical coordinates with a conformal factor. To change it to cylindrical coordinates, the required reparameterizations are,

$$\rho = \varrho \sin\theta \qquad\qquad \text{and} \qquad\qquad z = \varrho\cos\theta\,. \tag{4.42}$$

After incorporating the above changes, the Schwarzschild metric in isotropic cylindrical coordinates takes form,

$$\mathrm{d}s^2 = -\frac{\left(1-\frac{m}{2\sqrt{\rho^2+z^2}}\right)^2}{\left(1+\frac{m}{2\sqrt{\rho^2+z^2}}\right)^2}\mathrm{d}t^2 + \left(1+\frac{m}{2\sqrt{\rho^2+z^2}}\right)^4 (\mathrm{d}\rho^2 + \mathrm{d}z^2 + \rho^2\mathrm{d}\phi^2)\,. \tag{4.43}$$

4.3.2 Foliation of Spacetime and Two Dimensional Surfaces

The equation of a constant time hypersurface in isotropic cylindrical coordinates is given by,

$$t_\Sigma = \text{constant}\,, \tag{4.44}$$

where each slicing Σ_t is a spacelike three dimensional hypersurface. The induced metric on Σ_t is a conformally flat one,

$$h_{ij}\mathrm{d}x^i\mathrm{d}x^j = \left(1+\frac{m}{2\sqrt{\rho^2+z^2}}\right)^4 (\mathrm{d}\rho^2 + \mathrm{d}z^2 + \rho^2\mathrm{d}\phi^2)\,, \tag{4.45}$$

where lower case latin letters are hypersurface indices and $x^i = (\rho, z, \phi)$. The unit timelike normal to the slicing Σ_t is,

$$u_\alpha \mathrm{d}x^\alpha = -\frac{1-\frac{m}{2\sqrt{\rho^2+z^2}}}{1+\frac{m}{2\sqrt{\rho^2+z^2}}}\mathrm{d}t\,. \tag{4.46}$$

Like the standard Schwarzschild coordinates, here also the constant time slicing Σ_t is extrinsically flat,

$$K_{\alpha\beta} = \nabla_\alpha u_\beta = 0\,, \tag{4.47}$$

where ∇_α denotes covariant derivative with respect to the metric (4.43).

Any axisymmetric two dimensional surface $\mathcal{S}$ in Σ_t can be parameterized as,

$$\rho = P(\lambda)\,, \qquad z = Z(\lambda) \qquad \text{and} \qquad \phi = \phi\,, \tag{4.48}$$

for P and Z are some functions of λ. Incorporating the above reparameterization in (4.45), we get the induced metric on $\mathcal{S}$,

$$q_{AB}\mathrm{d}x^A\mathrm{d}x^B = \left(1 + \frac{m}{2\sqrt{P^2+Z^2}}\right)^4 ((P_\lambda^2 + Z_\lambda^2)\mathrm{d}\lambda^2 + P^2\mathrm{d}\phi^2)\,. \tag{4.49}$$

For $x^A = (\lambda, \phi)$ is two dimensional surface coordinate and subscript λ signifies derivative with respect to λ. The tangents to the surface $\mathcal{S}$ are,

$$\frac{\mathrm{d}}{\mathrm{d}\lambda} = P_\lambda \frac{\partial}{\partial\rho} + Z_\lambda \frac{\partial}{\partial z} \qquad \text{and} \qquad \frac{\partial}{\partial\phi}\,. \tag{4.50}$$

The unit spacelike normal to $\mathcal{S}$ is given by,

$$n = C\left(-Z_\lambda \frac{\partial}{\partial\rho} + P_\lambda \frac{\partial}{\partial z}\right)\,, \tag{4.51}$$

where

$$C = \left[\left(1 + \frac{m}{2\sqrt{P^2+Z^2}}\right)^4 (Z_\lambda^2 + P_\lambda^2)\right]^{-\frac{1}{2}}\,. \tag{4.52}$$

4.3.3 Expansions

As we already mentioned previously, the normal space of a spacelike two dimensional surface is timelike. Hence, the normal space of $\mathcal{S}$ can be spanned by two null normals.

Two such null normals are

$$\ell^+ = u + n \qquad \text{and} \qquad \ell^- = \frac{1}{2}(u - n). \tag{4.53}$$

The corresponding null expansions are

$$\theta^+ = q^{\alpha\beta}\nabla_\alpha \ell^+_\beta \qquad \text{and} \qquad \theta^- = q^{\alpha\beta}\nabla_\alpha \ell^-_\beta, \tag{4.54}$$

where

$$q^{\alpha\beta} = e^\alpha_i e^\beta_j q^{ij} = e^\alpha_i e^\beta_j e^i_A e^j_B q^{AB}. \tag{4.55}$$

Here e^α_i are the push forward/pullback operators between Schwarzschild spacetime and Σ_t and e^i_A are the push forward/pullback operator between Σ_t and surface $\mathcal{S}$.

Now,

$$\begin{aligned}
\theta^+ &= q^{\alpha\beta}\nabla_\alpha u_\beta + q^{ij}\nabla_i n_j \\
&= q^{\alpha\beta}K_{\alpha\beta} + q^{ij}\nabla_i n_j \\
&= q^{ij}\nabla_i n_j \\
&= q^{ij}k_{ij} \\
&= k.
\end{aligned} \tag{4.56}$$

and

$$\begin{aligned}
\theta^- &= \frac{1}{2}\left(q^{\alpha\beta}\nabla_\alpha u_\beta - q^{ij}\nabla_i n_j\right) \\
&= \frac{1}{2}\left(q^{\alpha\beta}K_{\alpha\beta} - q^{ij}\nabla_i n_j\right) \\
&= -\frac{1}{2}q^{ij}\nabla_i n_j \\
&= -\frac{1}{2}q^{ij}k_{ij} \\
&= -\frac{1}{2}k.
\end{aligned} \tag{4.57}$$

Here we used equation (4.47). k is the trace of extrinsic curvature of $\mathcal{S}$. Note that both expansions are proportional to k, similar to the Schwarzschild coordinates. This means the MOTOS will also be minimal surfaces for a vanishing k.

4.3.4 Equations of MOTOS

Similar to the Schwarzschild coordinate case, it is clear from (4.56) and (4.57) that the expansions in the both null directions vanish if $\mathcal{S}$ is a minimal surface. So, according to the definition of MOTOS, minimal surfaces in Σ_t are MOTOS in isotropic cylindrical coordinates. Therefore the equation of MOTOS is the minimal surface equation, which is

$$\begin{aligned} & k = e^i_A e^j_B q^{AB} \nabla_i n_j = 0 \\ \Longrightarrow\ & (P_{\lambda\lambda} - Z_{\lambda\lambda})(2\delta + m)\delta^2 - \left(\frac{2\delta^3}{P} + \frac{mZ^2}{P} - 3mP\right)(Z_\lambda^3 + Z_\lambda P_\lambda^2) \\ & + 4mZ(Z_\lambda^2 P_\lambda + P_\lambda^3) = 0\,, \end{aligned} \tag{4.58}$$

where $\delta = \sqrt{P^2 + Z^2}$ and

$$e^i_A = \frac{\partial x^i}{\partial x^A} = \begin{pmatrix} P_\lambda & 0 \\ Z_\lambda & 0 \\ 0 & 1 \end{pmatrix}. \tag{4.59}$$

For simplification, we work in the parameterization where $\lambda \equiv \rho$ and $Z = Z(\rho)$. This changes the above equation into,

$$Z_{\rho\rho}(2\epsilon + m)\epsilon^2 + \left(\frac{2\epsilon^3}{\rho} + \frac{mZ^2}{\rho} - 3m\rho\right)(Z_\rho^3 + Z_\rho) + 4mZ(Z_\rho^2 + 1) = 0\,, \tag{4.60}$$

where $\epsilon = \sqrt{\rho^2 + Z^2}$ and subscript ρ means derivative with respect to ρ.

As a second convenient parameterization, we take $\lambda \equiv z$ and $P = P(z)$. Putting this into (4.58), it will take the form,

$$P_{zz}(2\varepsilon + m)\varepsilon^2 - \left(\frac{2\varepsilon^3}{P} + \frac{mz^2}{P} - 3mP\right)(P_z^2 + 1) - 4mz(P_z^3 + P_z) = 0\,, \qquad (4.61)$$

where subscript z denotes $\partial/\partial z$ and $\varepsilon = \sqrt{P^2 + z^2}$. Next we will numerically solve these equations to find axisymmetric MOTOS in the isotropic cylindrical coordinate system.

4.3.5 Numerical Solution

In the isotropic cylindrical coordinate system, the integration of equation (4.60) (equation (4.61)) leads to the divergence problem where there is a local extremum in ρ (z). Similar to the Schwarzschild standard coordinate system, here also we will switch between equation (4.60) and equation (4.61) to counter it. We also study the behaviour of axisymmetric MOTOS that intersects z-axis perpendicularly. Note that both of these equations are not defined at the z-axis. However, we can always have a starting point that is very close to the z-axis.

Figure 4.6 shows the MOTOS approaching towards the horizon from above. Far from the horizon, they start from the z-axis and go to infinity maintaining their original order. As we get closer to the horizon, the z-intersecting surfaces start to curve more and more to wrap around the horizon before heading off to infinity. Very close to the horizon, the surfaces slowly diverge away to reach near the other side of the horizon and then take a turn to go to large ρ. The closer the starting point is to the horizon, the sharper the turn is and then it wraps around the horizon twice [see figure 4.7]. This process can be repeated an arbitrary number of times [13].

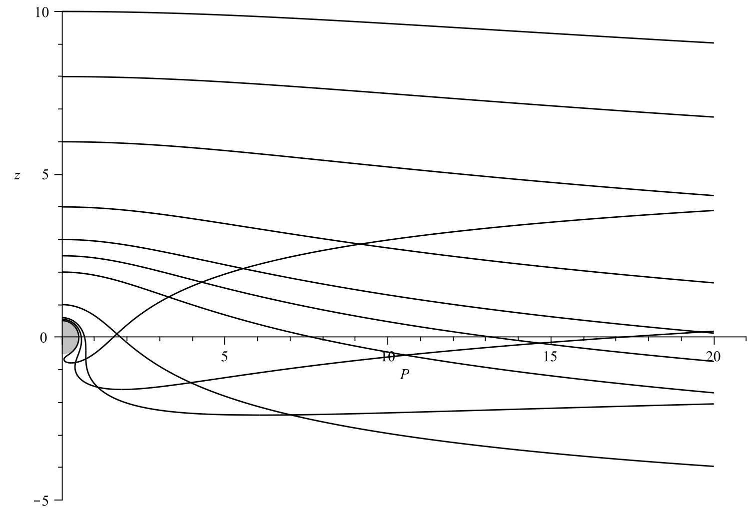

Figure 4.6: Minimal surfaces (MOTOS) that intersect the$z$-axis from above in isotropic cylindrical coordinate system. These were all integrated from the z-axis using the $Z(\rho)$ equation (4.60) and $P(z)$ from equation (4.61) alternatively.

The MOTOS with arbitrary number of folds wrapped around the horizon and then heading off to infinity.

4.4 MOT(O)S in Painlevé-Gullstrand Coordinates

Like the previous two coordinate systems, constant time slices in Painlevé-Gullstrand (PG) coordinates are spacelike. Hence any two dimensional surface in constant time hypersurfaces will also be spacelike. There are several advantages to working with PG coordinates compared to the previous two coordinate systems. PG coordinates are horizon-penetrating. It is possible to study trapped surfaces that cross the horizon. In this coordinate system, any constant time slicing is non-static. As a result, the expansion of spacelike two dimensional surfaces in the two null directions does not

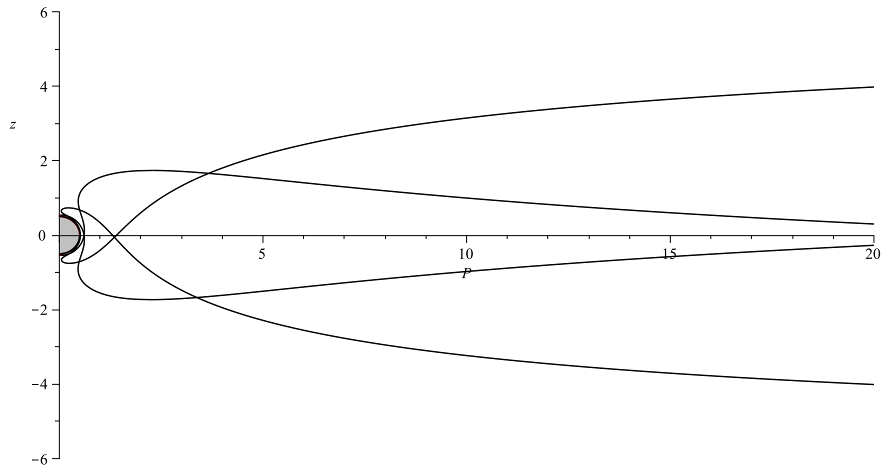

Figure 4.7: z-intersecting minimal surfaces (MOTOS) very close to the horizon in isotropic cylindrical coordinate system. These were all integrated from the z-axis using the $Z(\rho)$ equation (4.60) and $P(z)$ from equation (4.61) alternatively.

vanish simultaneously. Hence, it will be possible to study surfaces for which the expansions can vanish independently. Also the hypersurfaces of constant time are intrinsically Euclidean ($\mathbb{R}^3$). We can use Cartesian coordinates, $x = r\sin\theta$ and $z = r\cos\theta$ to describe the geodesics in a simpler way.

4.4.1 Metric

Standard Schwarzschild coordinates have a coordinate singularity at horizon. At $r = 2m$, the metric coefficient of $\mathrm{d}r^2$ blows up. To avoid that let us define a new time,

$$\tau = t - a(r)\,, \tag{4.62}$$

where $a = a(r)$ is some function of r. Putting it in (4.4), we get,

$$\begin{aligned} ds^2 = &- \left(1 - \frac{2m}{r}\right) d\tau^2 - 2\left(1 - \frac{2m}{r}\right) a'(r) d\tau dr \\ &+ \left(\frac{1}{\left(1 - \frac{2m}{r}\right)} - \left(1 - \frac{2m}{r}\right) a'^2(r)\right) dr^2 + r^2 d\theta^2 + r^2 \sin\theta^2 d\phi^2 \,, \end{aligned} \tag{4.63}$$

where

$$a'(r) \equiv \frac{da}{dr}$$

is the derivative of a with respect to r.

As a is an arbitrary function of r, we can choose it such a way that coefficient of dr^2 in (4.63) becomes unity then,

$$\left(\frac{1}{\left(1 - \frac{2m}{r}\right)} - \left(1 - \frac{2m}{r}\right) a'^2(r)\right) = 1 \,. \tag{4.64}$$

This requires

$$a'(r) = \frac{\sqrt{\frac{2m}{r}}}{\left(1 - \frac{2m}{r}\right)} \,. \tag{4.65}$$

Therefore,

$$\begin{aligned} a(r) &= \int \frac{da}{dr} \\ &= \frac{\sqrt{\frac{2m}{r}}}{\left(1 - \frac{2m}{r}\right)} \\ &= 2m\left(2\sqrt{\frac{r}{2m}} - \ln\frac{\sqrt{\frac{r}{2m}} + 1}{\sqrt{\frac{r}{2m}} - 1}\right) \,. \end{aligned} \tag{4.66}$$

So the metric becomes,

$$ds^2 = -\left(1 - \frac{2m}{r}\right) d\tau^2 + 2\sqrt{\frac{2m}{r}} d\tau dr + dr^2 + r^2 d\theta^2 + r^2 \sin\theta^2 d\phi^2 \,. \tag{4.67}$$

Note that at $r = 2m$, the metric (4.67) is regular.

4.4.2 Foliation and Curvature

As previous cases, here also we will consider a constant time spacelike hypersurface (Σ_τ), where $\tau =$ constant. The induced metric is a Euclidean one,

$$h_{ij} = \mathrm{d}r^2 + r^2(\mathrm{d}\theta^2 + \sin^2\theta\mathrm{d}\phi^2)\,, \tag{4.68}$$

where $x^i = (r, \theta, \phi)$ denotes the coordinates of hypersurface Σ_τ. In contrast to the spherical coordinate case, these constant time slices are intrinsically flat, not extrinsically. The timelike unit normal for the slices (Σ_τ) is

$$u = u_\alpha \mathrm{d}x^\alpha = -\mathrm{d}\tau\,. \tag{4.69}$$

In vector form,

$$u^\alpha \frac{\mathrm{d}}{\mathrm{d}x^\alpha} = \frac{\partial}{\partial\tau} - \sqrt{\frac{2m}{r}}\frac{\partial}{\partial r}\,. \tag{4.70}$$

The extrinsic curvature of the hypersurface is given by

$$\begin{aligned} K_{\alpha\beta} &= \nabla_\alpha u_\beta \\ &= \frac{\partial u_\beta}{\partial x^\alpha} - \Gamma^\gamma_{\alpha\beta} u_\gamma\,, \end{aligned} \tag{4.71}$$

where ∇_α denotes covariant derivative and $\Gamma^\gamma_{\alpha\beta}$ is the Christoffel symbol for the full metric (4.67). Running over (τ, r, θ, ϕ), the only non-zero components of Christoffel symbol are,

$$K_{rr} = \sqrt{\frac{m}{2r^3}}, \qquad K_{\theta\theta} = -\sqrt{2mr} \qquad \text{and} \qquad K_{\phi\phi} = -\sqrt{2mr}\sin^2\theta. \tag{4.72}$$

Now let us choose a constant time hypersurface, Σ_{τ_o} where $\tau = \tau_o$. Like the previous two cases, any axisymmetric two dimensional surface $\mathcal{S}$ in Σ_{τ_o} can be parameterized by (λ, ϕ) as

$$\tau = \tau_o\,, \qquad r = R(\lambda)\,, \qquad \theta = \Theta(\lambda) \qquad \text{and} \qquad \phi = \phi \tag{4.73}$$

for some functions $\Theta(\lambda)$ and $R(\lambda)$. Tangents to $\mathcal{S}$ are,

$$\frac{\mathrm{d}}{\mathrm{d}\lambda} = \dot{R}\frac{\partial}{\partial r} + \dot{\Theta}\frac{\partial}{\partial \theta} \qquad \text{and} \qquad \frac{\mathrm{d}}{\mathrm{d}\phi}, \tag{4.74}$$

where the dot denotes the derivative with respect to λ. The induced metric on $\mathcal{S}$ is

$$q_{AB}\mathrm{d}x^A\mathrm{d}x^B = (\dot{R}^2 + R^2\dot{\Theta}^2)\mathrm{d}\lambda^2 + (R^2\sin^2\Theta)\mathrm{d}\phi^2\,, \tag{4.75}$$

where upper case latin letters are $\mathcal{S}$ indices and run over $(\lambda,\, \phi)$. The unit spacelike normal to $\mathcal{S}$ in Σ_{τ_o} is given by,

$$\hat{r} = \frac{1}{\sqrt{\dot{R}^2 + R^2\dot{\Theta}^2}}\left(\dot{\Theta}\frac{\partial}{\partial r} - \frac{\dot{R}}{R^2}\frac{\partial}{\partial \theta}\right). \tag{4.76}$$

4.4.3 Null Expansions

The pair of null normals that span the timelike normal space of $\mathcal{S}$ are

$$\ell^+ = \hat{u} + \hat{r} \qquad \text{and} \qquad \ell^- = \frac{1}{2}(\hat{u} - \hat{r})\,. \tag{4.77}$$

The expansions associated with the null normals are given by,

$$\begin{aligned}
\theta^+ &= q^{\alpha\beta}\nabla_\alpha \ell^+_\beta \\
&= q^{\alpha\beta}\nabla_\alpha \hat{u}_\beta + q^{ij}\nabla_i \hat{r}_j \\
&= \theta_{(\hat{u})} + \theta_{(\hat{r})} \\
&= \theta_{(\hat{u})} + \theta_{(\hat{r})}\,,
\end{aligned} \tag{4.78}$$

and

$$\begin{aligned}\theta^{-} &= q^{\alpha\beta}\nabla_{\alpha}\ell^{-}_{\beta} \\ &= \frac{1}{2}(q^{\alpha\beta}\nabla_{\alpha}\hat{u}_{\beta} - q^{ij}\nabla_{i}\hat{r}_{j}) \\ &= \frac{1}{2}(\theta_{(\hat{u})} - \theta_{(\hat{r})}) \\ &= \frac{1}{2}(\theta_{(\hat{u})} - \theta_{(\hat{r})})\,, \end{aligned} \tag{4.79}$$

where

$$q^{\alpha\beta} = e^{\alpha}_{i} e^{\beta}_{j} q^{ij}\,. \tag{4.80}$$

In the above, $\theta_{(\hat{u})} \equiv q^{\alpha\beta}K_{\alpha\beta}$ is the trace of extrinsic curvature of $\mathcal{S}$ with respect to the timelike normal $\hat{u}$ and $\theta_{(\hat{r})} \equiv q^{ij}\nabla_{i}\hat{r}_{j}$ is the trace of extrinsic curvature of $\mathcal{S}$ in Σ_{τ_o}. The e^{α}_{i} are the push-forward operators from Σ_{τ} to the full spacetime,

$$e^{\alpha}_{i} = \frac{\partial x^{\alpha}}{\partial x^{i}} = \begin{pmatrix} 0 & 0 & 0 \\ 1 & 0 & 0 \\ 0 & 1 & 0 \\ 0 & 0 & 1 \end{pmatrix}\,, \tag{4.81}$$

and q^{ij} is the push-forward of the inverse surface metric into Σ_{τ},

$$q^{ij} = e^{i}_{A} e^{j}_{B} q^{AB} = h^{ij} - \hat{r}^{i}\hat{r}^{j}\,, \tag{4.82}$$

where

$$e^{i}_{A} = \frac{\partial x^{i}}{\partial x^{A}} = \begin{pmatrix} \dot{R} & 0 \\ \dot{\Theta} & 0 \\ 0 & 1 \end{pmatrix}\,. \tag{4.83}$$

Now,

$$\begin{aligned}\theta_{(\hat{u})} &\equiv q^{\alpha\beta}\nabla_\alpha \hat{u}_\beta \\ &= e^\alpha_i e^\beta_j q^{ij}\nabla_\alpha \hat{u}_\beta\,. \end{aligned} \tag{4.84}$$

Using (4.71) and then (4.82) we get,

$$\begin{aligned}\theta_{(\hat{u})} &= e^\alpha_i e^\beta_j q^{ij} K_{\alpha\beta} \\ &= e^\alpha_i e^\beta_j (h^{ij}) K_{\alpha\beta} - \hat{r}^i\hat{r}^j K_{\alpha\beta}) \\ &= \frac{\sqrt{2m}}{2R^{\frac{3}{2}}}\left(\frac{\dot{R}^2+4R^2\dot{\Theta}^2}{\dot{R}^2+R^2\dot{\Theta}^2}\right), \end{aligned} \tag{4.85}$$

and

$$\begin{aligned}\theta_{(\hat{r})} &\equiv q^{ij}\nabla_i \hat{r}_j \\ &= q^{ij}\frac{\partial \hat{r}_j}{\partial x^i} - q^{ij}\Gamma^k_{ij}\hat{r}_j \\ &= q^{AB}\frac{\partial x^i}{\partial x^A}\frac{\partial x^j}{\partial x^B}\frac{\partial \hat{r}_j}{\partial x^i} - q^{ij}\Gamma^k_{ij}\hat{r}_j \\ &= q^{\lambda\lambda}\left(\frac{\mathrm{d}}{\mathrm{d}\lambda}\right)^j \frac{\partial \hat{r}_j}{\partial \lambda} - q^{ij}\Gamma^k_{ij}\hat{r}_j \\ &= \frac{1}{\sqrt{\dot{R}^2+R^2\dot{\Theta}^2}}\left(\frac{R(\dot{R}\ddot{\Theta}-\ddot{R}\dot{\Theta})+\dot{\Theta}\dot{R}^2}{\dot{R}^2+R^2\dot{\Theta}^2} - \frac{\dot{R}\cot\Theta}{R} + 2\dot{\Theta}\right). \end{aligned} \tag{4.86}$$

Here Γ^k_{ij} denotes the Christoffel symbol with respect to the hypersurface metric (4.68).

Therefore,

$$\begin{aligned}\theta^+ =&\frac{1}{\sqrt{\dot{R}^2+R^2\dot{\Theta}^2}}\left(\frac{R(\dot{R}\ddot{\Theta}-\ddot{R}\dot{\Theta})+\dot{\Theta}\dot{R}^2}{\dot{R}^2+R^2\dot{\Theta}^2} - \frac{\dot{R}\cot\Theta}{R} + 2\dot{\Theta}\right) \\ &+ \frac{\sqrt{2m}}{2R^{\frac{3}{2}}}\left(\frac{\dot{R}^2+4R^2\dot{\Theta}^2}{\dot{R}^2+R^2\dot{\Theta}^2}\right). \end{aligned} \tag{4.87}$$

and

$$\theta^{-} = -\frac{1}{2\sqrt{\dot{R}^2 + R^2\dot{\Theta}^2}} \left(\frac{R(\dot{R}\ddot{\Theta} - \ddot{R}\dot{\Theta}) + \dot{\Theta}\dot{R}^2}{\dot{R}^2 + R^2\dot{\Theta}^2} - \frac{\dot{R}\cot\Theta}{R} + 2\dot{\Theta} \right)$$
$$+ \frac{\sqrt{2m}}{4R^{\frac{3}{2}}} \left(\frac{\dot{R}^2 + 4R^2\dot{\Theta}^2}{\dot{R}^2 + R^2\dot{\Theta}^2} \right). \qquad (4.88)$$

4.4.4 Equations of MOTOS

Unlike the previous cases, here the trace of extrinsic curvature of $\mathcal{S}$ with respect to the timelike normal, $\theta_{(\hat{u})}$ is non-zero. As a result, θ^{+} and θ^{-} do not vanish simultaneously. According to the definition of MOTOS, we are interested in surfaces for which the expansion associated to one of these two null normals vanishes. Thus the two possible equations for vanishing null expansions are:

$$\theta^{+} = \theta_{(\hat{u})} + \theta_{(\hat{r})} = 0, \qquad (4.89)$$

and

$$\theta^{-} = \frac{1}{2}(\theta_{(\hat{u})} - \theta_{(\hat{r})}) = 0$$
$$\Longrightarrow \theta_{(\hat{u})} - \theta_{(\hat{r})} = 0. \qquad (4.90)$$

Combining (4.89) and (4.90),

$$\theta_{(\hat{u})} \pm \theta_{(\hat{r})} = 0. \qquad (4.91)$$

That is,

$$\pm \left(\dot{R}\ddot{\Theta} - \ddot{R}\dot{\Theta} + \frac{3\dot{\Theta}\dot{R}^2}{R} - \frac{\dot{R}\cot\Theta}{R^2}(\dot{R}^2 + R^2\dot{\Theta}^2) + 2R\dot{\Theta}^3 \right)$$
$$+ \sqrt{\frac{m}{2}} \left(\frac{\sqrt{\dot{R}^2 + R^2\dot{\Theta}^2}(\dot{R}^2 + 4R^2\dot{\Theta}^2)}{R^{\frac{5}{2}}} \right) = 0. \qquad (4.92)$$

Solutions to both the equations (4.92) are equally important. What differs between the two cases is the orientation of the spacelike normal $\hat{r}$.

Like the previous two cases, using a coordinate parameterization makes the equations easier to work with. If we take $r = \lambda$, so that Θ becomes a function of r: $\Theta \equiv \Theta(r)$. Then (4.92) becomes,

$$\begin{aligned}\Theta_{\pm}^{\text{Eq}}: \quad \Theta_{rr} + \frac{3\Theta_r}{r} - \frac{\cot\Theta}{r^2}\left(1 + r^2\Theta_r^2\right) + 2r\Theta_r^3 \\ \mp\sqrt{\frac{m}{2}}\frac{\sqrt{1+r^2\Theta_r^2}\,(1+4r^2\Theta_r^2)}{r^{5/2}} = 0\,. \end{aligned} \tag{4.93}$$

where the subscript r denotes the derivative with respect to r and

$$\hat{r} = \frac{r}{\sqrt{1+r^2\Theta_r^2}}\left(\Theta_r\left(\frac{\partial}{\partial r}\right) - \frac{1}{r^2}\left(\frac{\partial}{\partial\theta}\right)\right). \tag{4.94}$$

We can do a similar coordinate parameterization for θ. Consider $\lambda = \theta$, which means $R \equiv R(\theta)$. In this parameterization (4.92) becomes,

$$\begin{aligned}R_{\pm}^{\text{Eq}}: \; R_{\theta\theta} - \frac{3R_\theta^2}{R} + \frac{R_\theta\cot\theta}{R^2}\left(R_\theta^2 + R^2\right) - 2R \\ \pm\sqrt{\frac{m}{2}}\frac{\sqrt{R_\theta^2+R^2}\,(R_\theta^2+4R^2)}{R^{5/2}} = 0\,. \end{aligned} \tag{4.95}$$

where subscript θ denotes derivative with respect to θ and

$$\hat{r} = \frac{R}{\sqrt{R_\theta^2+R^2}}\left(\left(\frac{\partial}{\partial r}\right) - \frac{R_\theta}{R^2}\left(\frac{\partial}{\partial\theta}\right)\right). \tag{4.96}$$

Note that in total we have four MOT(O)S equations: two for each parameterization. As mentioned before due to non-static property of PG coordinates, expansions along ℓ^+ and ℓ^- do not vanish simultaneously. The R_+^{Eq} and Θ_+^{Eq} equations correspond to MOTOS with vanishing expansion along ℓ^+, whereas the MOTOS with vanishing expansion along ℓ^- is represented by R_-^{Eq} and Θ_-^{Eq}. Also the orientation of $\hat{r}$ is linked to the parameterizations (4.73). If we change the parameterizations, the orientation of $\hat{r}$ also changes. For $\lambda = \theta$ parameterization, $\hat{r}$ given by (4.96) points towards the positive r direction, while $\hat{r}$ in $\lambda = r$ parameterization (given by (4.94)) is directed towards negative θ. As a result, the null directions ℓ^+ and ℓ^- also change. For all four equations, the directions of vanishing null expansion are different. So, in order to maintain a consistent "outward" direction along the full MOT(O)S, we need to switch back and forth between all four equations.

Another reason for switching back and forth between $R_\pm^{\mathrm{Eq}}$ and $\Theta_\pm^{\mathrm{Eq}}$ is to avoid running into a coordinate singularities. This procedure is similar to the one we discussed in the beginning of subsection 4.2.5. These infinities occur when the surface becomes tangent to either ∂_r or ∂_θ.

4.4.5 Analytical Results

Before diving into the numerical findings, we will explore some analytical results. Our aim is to find constraints on possible behaviours of those numerical solutions.

4.4.5.1 Minkowski Limit $m = 0$:

For $m = 0$, the metric (4.67) becomes Minkowski metric and the constant time slice Σ_t turns into a Euclidean $\mathbb{R}^3$ space. Also $\theta_{\hat{u}}$ from (4.92) vanishes for $m = 0$. Here again the problem boils down to solving $\theta_{\hat{r}} = 0$. That is, to find axisymmetric minimal surfaces in Euclidean $\mathbb{R}^3$. This is exactly the same situation that we encountered in the standard Schwarzschild coordinate system. The solution is a catenoid and this can be shown by directly substituting these parameterized equations of catenoid (4.30), (4.31) into the MOTOS equations in PG coordinates, i.e., equation (4.92) with

$m = 0$.

4.4.5.2 Intersections with z-axis

To find out if there is any MOTOS that intersects with the z-axis, we need to check whether or not any point on the axis will satisfy either (4.93) or (4.95). However there is a subtlety here because these equations include a term $\cot\theta$ which blows up at $\theta = 0, \pi$. Strictly speaking, this means these equations are not defined on the z-axis in general. However, we found such analytic surfaces do exist. $R(\theta)$ can be engineered to compensate for the "blow up" resulting in a well-defined solution. This can be done by obtaining a Taylor series expansion of $R(\theta)$ around $\theta = 0$ (or $\theta = \pi$) that satisfies (4.95). The idea is to substitute Taylor expansion of $R(\theta)$ around $\theta = 0$ into (4.95) and then solve it order-by-order. To ensure there is no blow up, we set, $R'(\theta)$ to zero. This is true if and only if the surfaces intersect z-axis perpendicularly. Around $\theta = 0$, the series found to be

$$R_0^{\pm}(\theta) = R_o + \frac{\sqrt{R_o}(\sqrt{R_o} \mp \sqrt{2m})}{2}\theta^2 + \mathcal{O}(\theta^4), \tag{4.97}$$

where R_0^+ and R_0^- are series expansion for vanishing null normal ℓ^+ and ℓ^- respectively. Note that here surface normal $\hat{r}$ points towards positive r. The expansion coefficients are same for $\theta = \pi$.

If we consider ℓ^+ as the outward normal, the corresponding series expansion around $\theta = 0, \pi$ is R_0^+. For R_0^+ expansion, $R_o = 2m$ is a solution. It confirms the obvious fact that the horizon is a MOTS. However, it is interesting to observe that for $R_o > 2m$, R_0^+ increases whereas for $R_o < 2m$, R_0^+ decreases. By contrast, for all inward oriented normals, R_0^- increases as the surface moves away from $\theta = 0, \pi$.

4.4.5.3 Local Extrema

Extrema of $R(\theta)$: For an extremum at $\theta = \theta_o$, we have $R(\theta_o) = R_o$, and $R_\theta(\theta_o) = 0$. Now, using these with (4.95), we find,

$$R_{\theta\theta}(\theta_o) = 2\sqrt{R_o}(\sqrt{R_o} \mp \sqrt{2m}). \tag{4.98}$$

Here the $-/+$ sign stands for surfaces of vanishing outward/inward oriented null expansions. For $m = 0$, $R_{\theta\theta}$ is always positive, so only minima are possible. It agrees with our analysis in section 4.4.5.1. This can also be seen in figure 4.2: the hyperbola has a minimum but no maximum in R.

For the general case, $R_{\theta\theta}$ is always positive for surfaces with inward oriented vanishing null expansion. Such surfaces can have only minima. On the other hand, for MOTOS with outward oriented vanishing null expansion, the situation is not so trivial. These surfaces can have minima at $R_o > 2m$ while $R_o < 2m$ can only be a local maximum. $R_o = 2m$ is a saddle point as $R_{\theta\theta}$ vanishes at this point.

The fact that there is no maximum in R outside of $R = 2m$ confirms all closed axisymmetric MOTSs inside the horizon stay in the black hole region [58]. This also matches with our analysis in section 4.4.5.2. There we found for the outward oriented surfaces that intersect z-axis, $R(\theta)$ increases for $R_o > 2m$. It resonates with the fact that there is no maximum in R outside $R_o = 2m$. Likewise, $R(\theta)$ decreases for $R_o < 2m$ agrees with $R_o < 2m$ being a possible maxima only.

Extrema of $\Theta(r)$: For an extremum $\Theta(r_o) = \Theta_o$, the first derivative vanishes,

$$\Theta_r(r_o) = 0\,. \tag{4.99}$$

Using the above value of Θ, Θ_r in equation (4.93), we get,

$$\Theta_{rr}(r_o) = \frac{1}{r_o^2}\left(\cot\Theta_o \pm \sqrt{\frac{m}{2r_o}}\right) . \tag{4.100}$$

Here, the $+/-$ sign denotes for the surfaces the direction of vanishing null expansion is towards $\theta = 0/\theta = \pi$.

From equation (4.100), it is clear that for $m = 0$, Θ_{rr} depends on $\cot\Theta_o$. Hence, extrema can be minima for $0 < \Theta_o < \pi/2$ as $\cot\Theta_o$ is positive in this range of Θ_o. This is in contrast with the range $\pi/2 < \Theta_o < \pi$, where Θ_{rr} is negative and only maxima are possible. Note that this agrees with the catenoid solution in the flat case. The value of Θ starts from a finite value within the range of $0 < \Theta_o < \pi/2$, which is the minimum and then Θ increases as it moves towards z-axis. The moment it crosses $\Theta = \pi/2$, it turns around and again heads towards a maximum value in the range of $\pi/2 < \Theta_o < \pi$ [see figure 4.2].

For the general case, the situation is more complex. For upward oriented (vanishing null expansion towards $\theta = 0$) surfaces, the second term in the right hand side of equation (4.100) is always positive. These surfaces for $0 < \Theta_o < \pi/2$ can only have minima as $\cot\Theta_o$ is positive in this range. On the other hand, $\cot\Theta_o$ is negative for $\pi/2 < \Theta_o < \pi$. So in the latter range, these surfaces can have both: minima if $|\cot\Theta_o| < \sqrt{m/2r_0}$ and maxima if $|\cot\Theta_o| > \sqrt{m/2r_0}$. However, $|\cot\Theta_o| = \sqrt{m/2r_0}$ are saddle points for these surfaces in the range $\pi/2 < \Theta_o < \pi$. For surfaces with downward orientation (direction of vanishing null expansion is along $\theta = \pi$) for $0 < \Theta_o < \pi/2$, also can have maxima if $|\cot\Theta_o| < \sqrt{m/2r_0}$, otherwise maxima except two saddle points, i.e. $|\cot\Theta_o| = \sqrt{m/2r_0}$. By contrast, for $\pi/2 < \Theta_o < \pi$, there is only a maxima as both the terms on the right hand side of equation (4.100) are negative.

4.4.5.4 Asymptotic Limit

For $m = 0$: For $R(z)$ and $\Theta(z)$ from equations (4.30) and (4.31) respectively, neither of them admits a simple inversion which would provide a simple expression $R(\theta)$ or $\Theta(r)$. However asymptotically for large r we can invert (4.30) and get,

$$z_{\mathrm{m=0}} = \mp \rho_o \left(X - \frac{2X^2+1}{4} \left(\frac{\rho_o}{r}\right)^2 + \mathcal{O}\left(\frac{\rho_o^4}{r^4}\right) \right), \tag{4.101}$$

where

$$X = \frac{z_o}{\rho_o} + \ln\left(\frac{2r}{\rho_o}\right). \tag{4.102}$$

In the above, the sign $-/+$ is for the the upper/lower branch of the catenoid ($-$ upper, $+$ lower). Here as r goes to infinity, all the terms except first one goes to zero.

$$\begin{aligned}\lim_{r\to\infty} z_{\mathrm{m=0}} &= \mp\rho_o \lim_{r\to\infty} X \\ &= \infty. \end{aligned} \tag{4.103}$$

We see that the $z_{\mathrm{m=0}}$ diverges logarithmically. Now substituting (4.101) in (4.93) and then asymptotically expanding it, we obtain,

$$\begin{aligned}\Theta_{\mathrm{m=0}}(r) = \frac{\pi}{2} \mp &\left(X\left(\frac{\rho_o}{r}\right) + \frac{2X^3 - 6X^2 - 3}{12}\left(\frac{\rho_o}{r}\right)^3 \right) \\ &+ \mathcal{O}\left(\frac{\rho_o^5}{r^5}\right), \end{aligned} \tag{4.104}$$

Clearly for $r \to \infty$, $\Theta_{\mathrm{m=0}}$ becomes $\pi/2$.

General case: To study the behaviour far from the black hole, we will asymptotically expand $\Theta(r)$ for large r and substitute it into (4.93). We will then solve it order-by-order. The challenging part here is to guess the correct ansatz for the asymptotic expansion. For $m \neq 0$, it is not unreasonable to expect that the MOTS will behave similar to that of $m = 0$ case asymptotically. However this is not the case. The ansatz used in the $m = 0$ case no longer works when $m \neq 0$. By trial and error method, we found that large r-limit solution is possible using an ansatz containing half powers of r and $\ln r$.The asymptotic series solutions to $\Theta^{Eq}_{\pm}$ (4.93) for $m > 0$ is found to be

$$\Theta^{\pm}_{\text{asympt}} = \frac{\pi}{2} \pm 2\sqrt{2}\left(\frac{m}{r}\right)^{1/2} + \tilde{X}\left(\frac{\beta}{r}\right) \mp \frac{10\sqrt{2}}{3}\left(\frac{m}{r}\right)^{3/2}$$

$$+ (3\tilde{X} - 7)\left(\frac{\beta m}{r^2}\right) + \mathcal{O}\left(\frac{m^i \beta^j}{r^{5/2}}\right), \tag{4.105}$$

where $i + j = 5/2$ and

$$\beta\tilde{X} = \alpha + \beta \ln r\,, \tag{4.106}$$

with each solution having distinct values of the constants, α and β. Note that similar to the $m = 0$ case,

$$\lim_{r\to\infty} \Theta^{\pm}_{\text{asympt}} = \frac{\pi}{2}. \tag{4.107}$$

Also the term associated with $1/r$ matches with the flat case (4.104) but only for upper branch of catenoid. In the previous case i.e. for $m = 0$, the leading term after $\pi/2$ in (4.104) is a $1/r$ term, whereas in general case, it is a $r^{-\frac{1}{2}}$ term. This difference is clearer for asymptotic z series,

$$z^{\pm}_{\text{asympt}} = r\cos\Theta^{\pm}_{\text{asympt}} \approx \pm 2\sqrt{2m}\, r^{1/2} - \beta\tilde{X} + \mathcal{O}(r^{-1/2})\,. \tag{4.108}$$

Note that the leading order $\sqrt{r}$ term does not depend on any constants, so it is same for all the the solutions. While it is true that for both the general case and the flat case, z diverges asymptotically, it is also true that it diverges as $\sqrt{r}$ for general case where for flat case it diverges logarithmically.

4.4.5.5 Behaviour near $r = 2m$

We know that $r = 2m$ is a MOTS with the expansion vanishing in the radially outward direction. To study the behaviour of MOT(O)S very close to $r = 2m$, we will try to find perturbative solutions to equation (4.95) of the form,

$$R(\theta) = 2m\left(1 + \rho(\theta)\right), \tag{4.109}$$

for $|\rho| \ll 1$. If we put the above expression into (4.95), then up to first order the equation will be,

$$R^{+}_{\mathrm{eq}} : \rho_{\theta\theta} + \cot\theta\rho_{\theta} - \rho = 0 \tag{4.110}$$

$$R^{-}_{\mathrm{eq}} : \rho_{\theta\theta} + \cot\theta\rho_{\theta} - 3\rho = 4 \tag{4.111}$$

where equation with $+$ $(-)$ denotes MOT(O)S with the same (opposite) vanishing null orientation to that of $r = 2m$. Solutions for these equations can be expressed in terms of a combination of Legendre functions and associated Legendre functions,

$$\rho^{+} = A^{+}P_{l^{+}}(\cos\theta) + B^{+}Q_{l^{+}}(\cos\theta), \tag{4.112}$$

$$\rho^{-} = -\frac{4}{3} + A^{-}P_{l^{-}}(\cos\theta) + B^{-}Q_{l^{-}}(\cos\theta) \tag{4.113}$$

where P_l and Q_l are Legendre and associated Legendre functions respectively. $A^{\pm}$ and $B^{\pm}$ are free constants and

$$l^{+} = -\frac{1 + i\sqrt{3}}{2} \quad \text{and} \quad l^{-} = -\frac{1 + i\sqrt{11}}{2}\,. \tag{4.114}$$

Here we are interested in MOT(O)S that intersects the positive z-axis perpendicularly very close to the horizon. From equation (4.109) we can say for these surfaces,

$$\rho \to \rho_o \qquad \text{and} \qquad \rho_\theta \to 0 \tag{4.115}$$

as $\theta \to 0$. For these conditions (4.115), the solutions of $R^{\pm}_{\text{eq}}$, (4.112) and (4.113) take the forms,

$$\rho^+ = \rho_o P_{l^+}(\cos\theta), \tag{4.116}$$

$$\rho^- = -\frac{4}{3} + \left(\frac{4}{3} + \rho_o\right) P_{l^-}(\cos\theta). \tag{4.117}$$

The constants $B^{\pm}$ in front of the associated Legendre function terms are required to be zero to have a well-defined solution as $\theta \to 0$. This perturbative solution leads to important conclusions. For MOT(O)S that intersects z-axis at $z = 2m$, (4.109) becomes $R(0) = 2m$, and that implies

$$\rho(0) = \rho_o = 0. \tag{4.118}$$

From (4.116), it is clear that for a MOT(O)S with $\rho_o = 0$, $\rho^+ = 0$. This is nothing but the $r = 2m$ MOTS itself. This is consistent with the uniqueness theorem for MOT(O)S [2, 39] that says two MOT(O)S that touch with the same orientation of their directions of vanishing null expansion must be identical. Also as the Legendre functions diverges at $\theta = \pi$, MOT(O)S with $\rho_o \neq 0$ will also diverges near negative z-axis.

4.4.6 Numerical Results

We will discuss numerical results here. We will follow the same method, we used in Schwarzschild and isotropic cylindrical coordinates. The only difference is here we

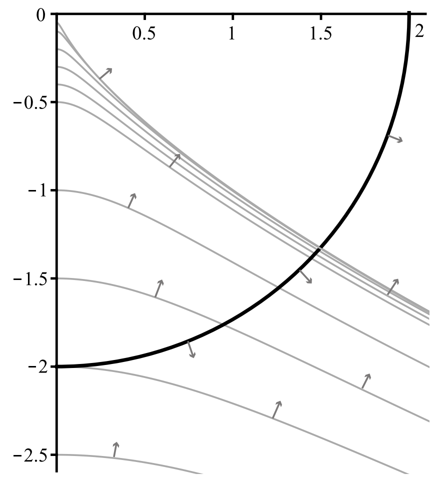

Figure 4.8: Axisymmetric MOTOS that intersect the negative z-axis moving close to $r = 2m$ from below and inside of it in a constant time slice of Schwarzschild spacetime in PG coordinate system. The arrows indicate the orientation of vanishing null expansion. The horizon is represented by the thick black line.

will use four equations instead of two. The procedure is similar to what is already discussed in subsection 4.4.4. We will integrate (4.93) and (4.95) to study axisymmetric MOT(O)S that intersect the positive z-axis at $z = z_o$ with vanishing null expansion oriented towards the positive z direction. As the PG coordinates can penetrate the horizon, we will able to study MOT(O)Ss across the horizon. Due to the reflectional symmetry of the surfaces around the z-axis, it is sufficient to study the MOT(O)S within the range $0 \leq r \sin\theta < \infty$ to understand the full surface.

Figure 4.8 shows the MOTOS that intersects the z-axis at $z_o < 0$ with the upward oriented (towards $\theta = 0$ or $+z$ direction) vanishing null expansion. These MOTOS are very simple in nature. They start from the negative z-axis to move (mostly horizontally) towards the large-r. They maintain their original ordering with which

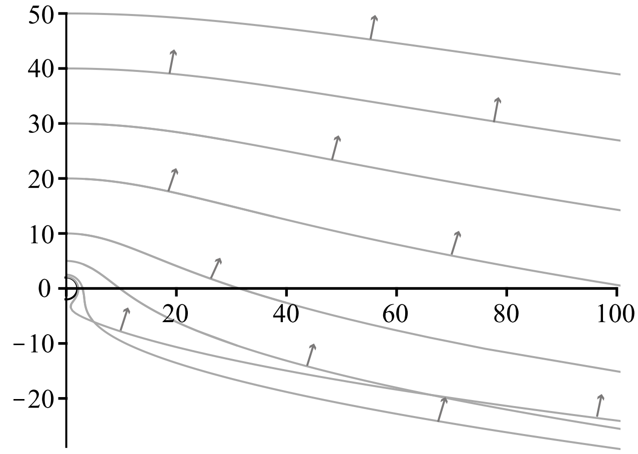

Figure 4.9: Axisymmetric MOTOS that intersect the positive z-axis approaching to $r = 2m$ from above in a constant time slice of Schwarzschild spacetime in PG coordinate system. The arrows indicate the orientation of vanishing null expansion. The horizon is represented by the thick black line.

they start from z-axis. This agrees with what we have discussed regarding extrema of $R(\theta)$ previously. The orientation of vanishing null expansion for these MOTOS is radially inward, so they cannot have any maxima.

Axisymmetric MOTOS with upward oriented vanishing null expansion, that intersect the positive z-axis at $z_o \geq 2m$ are shown in figure 4.9. These surfaces do not necessarily maintain their initial order from which they started with at z-axis. As they approach $r = 2m$, the surfaces become increasingly curved and more sharply wrap around the horizon $r = 2m$. At the end of this continuous process, at $z_o = 2m$ a (closed) MOTS forms that intersects the negative z-axis at $-2m$ perpendicularly. In other words, the $z_o = 2m$ MOTS coincides with the horizon $r = 2m$, which is also a MOTS. Note that this is consistent with the uniqueness theorem for MOTS. This is

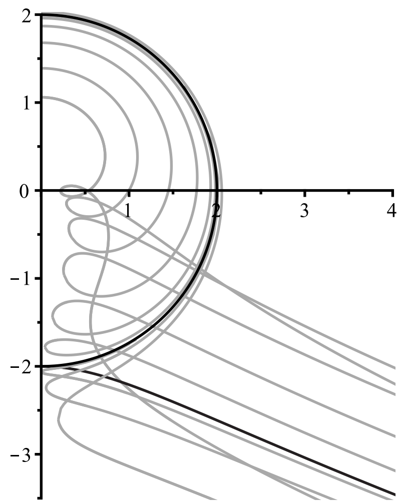

Figure 4.10: Axisymmetric self-intersecting MOTOS with one loop that intersect the positive z-axis inside $r = 2m$ in a constant time slice of Schwarzschild spacetime in PG coordinate system. The $r = 2m$ MOTS is represented by the thick black line.

because they touch each other with the same orientation of vanishing null expansion at $z_0 = 2m$. The axisymmetric upward oriented MOTOS that intersects z-axis at $z_o = -2m$ is tangent to the $z_o = 2m$ MOTS but has opposite orientation of vanishing null expansion at $z_o = -2m$. They pair together to form a limiting surface at the end of the continuous process we mentioned earlier. The $r = 2m$ MOTS can be seen in figure 4.10. The MOTOS that are very close to the horizon after wrapping around the $r = 2m$ turn around more and more sharply to avoid $\theta = \pi$ and then head off to infinity. This is expected and consistent with our previous analysis.

MOTOS that intersect the z-axis inside the horizon (at $z_o < 2m$) have similar trends. From z-axis they curve inside the $r = 2m$ and turn around near the $\theta = \pi$. Whereas the MOTOS outside $r = 2m$ turn to their left to avoid bumping into the negative z-axis, the MOTOS inside it turn to their right. They self-intersect to create a loop before going out of the $r = 2m$ surface and moving off to infinity. This behaviour can be seen in figure 4.10. Initially as z_o decreases, the loop created by the corresponding MOTOS becomes larger, moving further from $r = 2m$ and getting closer to the x-axis. After a point, the area of the loop decreases as it moves closer to the x-axis and the free end starts to curve towards the z-axis again before moving out of the $r = 2m$ surface. This continues with the free end pulling back towards z-axis more and more sharply until $z_o \approx 1.37m (= z_1)$. At this limit, the free end is no longer free end anymore: it intersects the z axis at $-z_1$ and so the surface has closed to become a MOTS. Interestingly, the loop of this limiting surface is symmetrically divided by the x-axis and the self-intersection point coincides with the x-axis. Figure 4.11 has shown this MOTS with one loop.

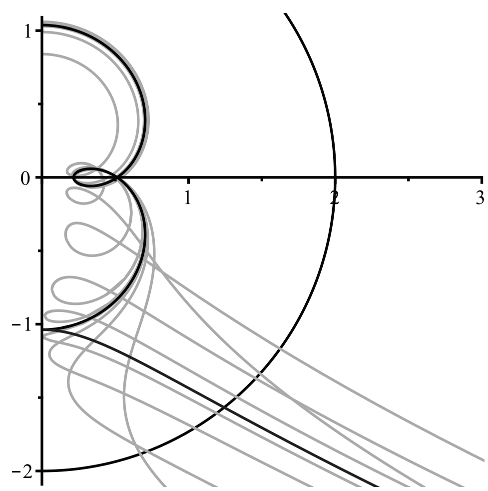

Figure 4.11: Axisymmetric self-intersecting MOTOS on the either side of one-loop MOTS in a constant time slice of Schwarzschild spacetime in PG coordinate system. MOTOS that intersect the positive z-axis inside one-loop MOTS develops a second loop before moving out of it.

For $z_o < z_1$, a new loop forms and the process repeats itself as we go deeper. At $z_o \approx 0.766 (= z_2)$ another limiting surface which is a MOTS appears with its two loops placed symmetrically from the x-axis with one loop on each side of the axis. This process repeats infinitely and the result is an infinite family of MOTS characterized by their number of self-intersections placed symmetrically around x-axis. The first twelve MOTS are shown in figure 4.12. If we follow the same notation then we can say that the i-th MOTS appear to intersect the z-axis at $z = \pm z_i$. Note that for any value of i, $z_{i+1} - z_i$ decreases as value of i increases.

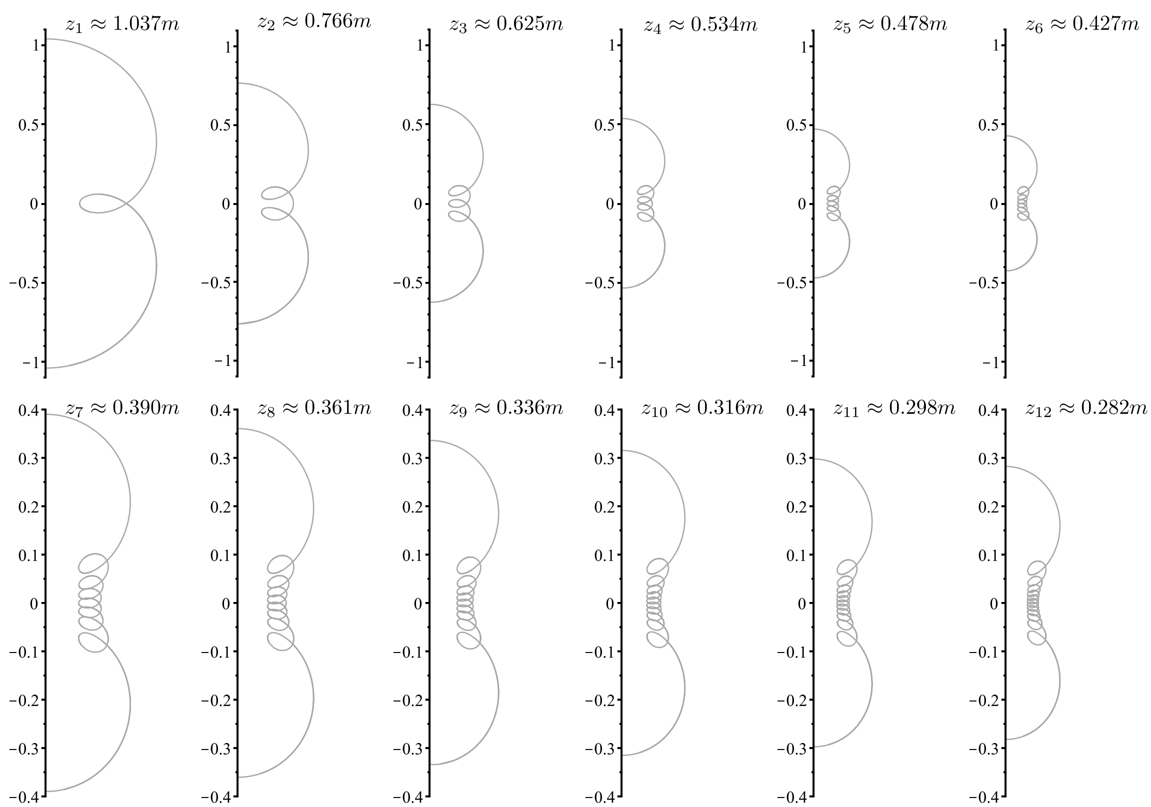

Figure 4.12: The first twelve MOTS inside the $r = 2m$ horizon in a constant time slice of Schwarzschild spacetime in PG coordinate system.

4.5 MOTS During Extreme Mass Ratio Mergers

Working in the PG coordinate system, we found some interesting self-intersecting MOT(O)S that are axisymmetric around the z-axis. As we mentioned already, during extreme mass ratio mergers close to the small black hole, the spacetime is approximated by the Schwarzschild spacetime. So, it is only logical to expect that the behaviour of MOTS during extreme mass ratio mergers will be close to that of MOT(O)S in the Schwarzschild geometry locally. The numerical results we found in the last section can be used to learn the behaviour of MOTS during EMR mergers. Of course it still remains to determine which ones are the correct surfaces and at what order they should be arranged. The ideal scenario would be solving the partial differential equations for the marginally outer trapped tube (MOTT). Given an initial MOTS, this solution would determine the future time evolution of that MOTS. While these equations could be very useful in scenarios such as this one and also can be extended to MOTOS, it is also true that finding solution to these differential equations is a highly non-trivial business. Here in this section, we speculate on the correct surfaces and their evolution with the help of our analytical and numerical results, based on contemporary studies [39, 46, 47, 8, 60, 33, 15, 14, 26].

Figure 4.13 shows the evolution of large and small black hole MOTS to the point where they touch each other. In a), the MOTS for the small black hole is represented by $r = 2m$ MOTS and the large black hole MOTOS has orientation with vanishing null expansion towards it. The MOTOS here resembles the MOTOS in PG coordinates (in 4.9) that intersects the z-axis far above the $r = 2m$ MOTS. They are getting closer in b). Note that the MOTOS below deforms more as it moves closer to the

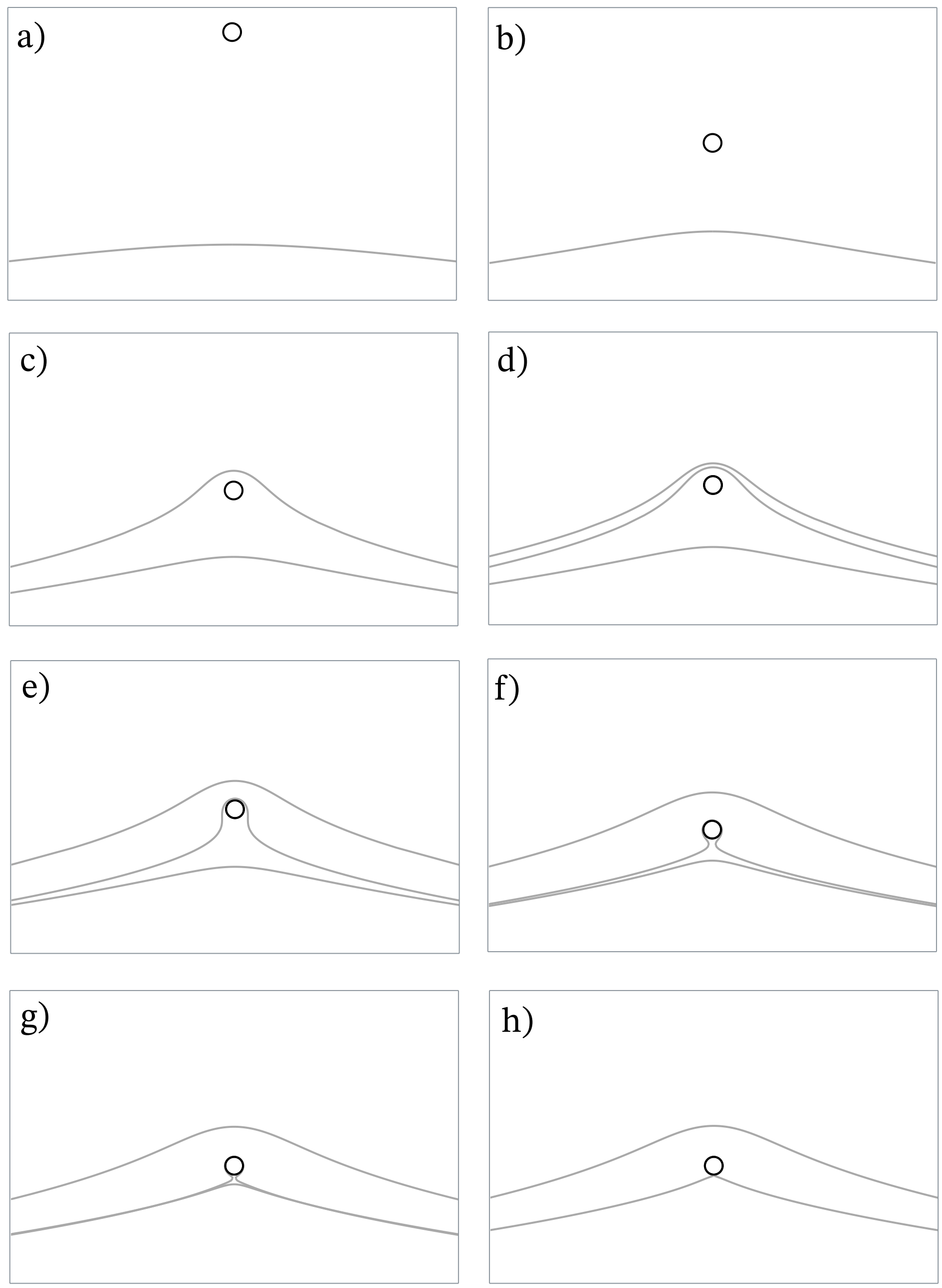

Figure 4.13: Possible constant time slices of evolving MOTS during the early stages of extreme mass ratio mergers in the chronological order. This is an informed speculation where we assembled the MOT(O)S (observed in Schwarzschild geometry) manually without any rigorous derivation.

small MOTS. This behaviour agrees with the observations in [39, 46, 47].

In $c)$ the MOTOS that originally represents the large black hole, jumps over and engulfs the small MOTS. Then the MOTOS bifurcates into two, one outer and one inner in $d)$.The interesting process of bifurcation of the MOTOS is also consistent with contemporary studies [39, 46, 47]. Similar horizon jumps are observed in [46, 47, 8, 60, 33, 15, 14, 26].

After that, the inner MOTOS gradually evolves to wrap around the $r = 2m$ MOTS more and more tightly until it coincides with the $r = 2m$ MOTS plus the original MOTOS for the large black hole. On the other hand, the outer one is getting more and more flat as seen in $e) - h)$ of figure 4.13. This is in line with the behaviour seen in [46, 47, 33].

The evolution of the surfaces beyond the point where the small black hole MOTS and the inner MOTOS touch is depicted in figure 4.14. Remember the self-intersecting MOTS with i loops that intersects the z-axis at $z = \pm z_i$ in last section. These MOTS plus the $z_o < 0$ upward-oriented MOTOS that intersect at $z = -z_i$ are the limiting surfaces to all the $z_o > 0$ upward-oriented MOTOS with i loops approaching to $z = +z_i$. This is only possible if the MOTS with i loops and the upward-oriented MOTOS that intersects at $z = -z_i$ reaches $z = z_i$ at the same time. Assuming this is true, we propose that after the inner MOTOS and $r = 2m$ coincide, the inner MOTOS contracts and move inside $r = 2m$. As $z_o \to 0$, the inner MOTOS develops more and more loops and the loops get closer and smaller. Along the way, as the loop grows the inner MOTOS alternatively keep intersecting the $z = -z_i$'s and then get away from the negative z-axis, creating one more loop at the same time. At the same time far from singularity the inner MOTOS approach the same limit surface as the

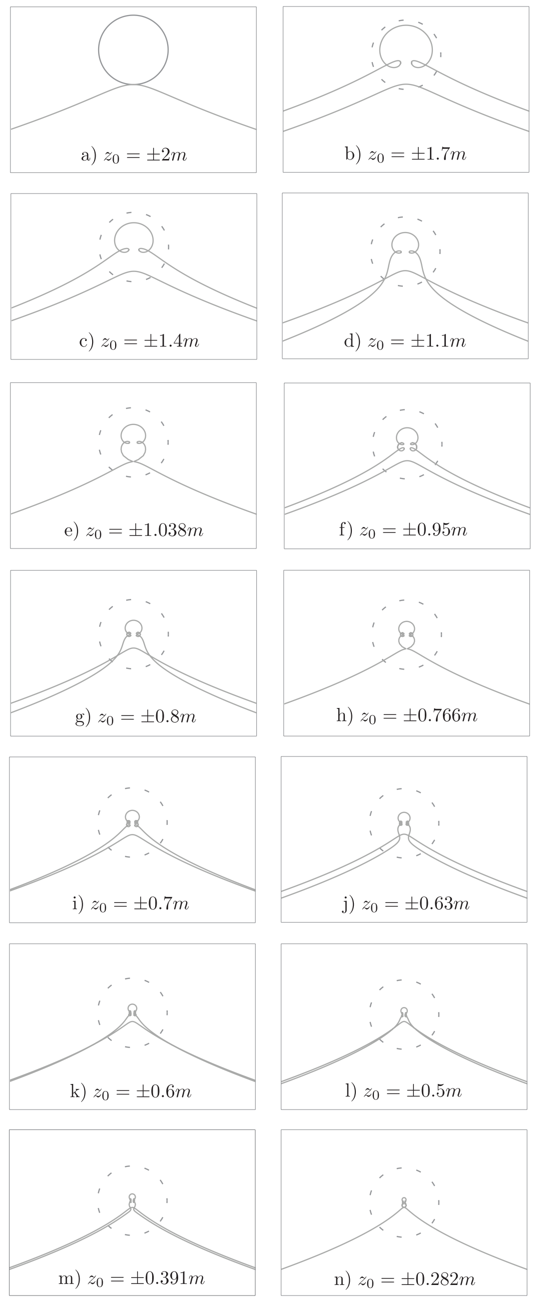

Figure 4.14: Possible constant time slices of evolving MOTS during the later stages of extreme mass ratio mergers in the chronological order. This is an informed speculation where we assembled the MOT(O)S (observed in Schwarzschild geometry) manually without any rigorous derivation.

original MOTOS representing the large black hole as $z_o \to 0$. On the other hand, the outer MOTOS from figure 4.13 continues to relax down and approaches to become a plane.

Chapter 5

Conclusions

In this project, we have studied axisymmetric MOT(O)S in a constant time slice in the Schwarzschild spacetime for three different coordinate systems. For the first two coordinate systems, that is standard Schwarzschild coordinates and isotropic cylindrical coordinates, the time slices are extrinsically flat, so the MOTOS in a time slice are minimal surfaces in these coordinate systems. This fact implies that for MOTOS, the expansion scalars along outward and inward null directions vanish simultaneously which means any two MOTOS that are tangent to each other are identical. Also these two coordinate systems are not horizon-penetrating. As a result, we are only able to study MOTOS outside horizon. In each case, MOTOS that begin very close to the horizon, can have arbitrary number of folds wrapped around the horizon before the heading off to infinity [13]. This is more clearly visible in the isotropic cylindrical coordinate system. The results we have obtained here are commensurate with [31].

Next, we considered the behaviour of MOTOS in the Painlevé-Gullstrand coordinate system. A key advantage of this coordinate system is that it is horizon-penetrating. As a result, we were able to study the behaviour of MOTOS that cross the black hole horizon. The time slices in this coordinate system are non-static in the sense that there is no degeneracy between vanishing expansion scalar along two null directions for MOT(O)S. In other words, the expansions along the outward and the inward directions are independent. We have studied MOT(O)S across the horizon and found an infinite family of self-intersecting MOT(O)S inside horizon with arbitrary number of loops.

Self-intersecting MOTS inside the Schwarzschild horizon have not been previously observed. However, similar MOTS have recently been shown to play a role in understanding black hole mergers [39, 46, 47] where a surface with a single self-intersection was found in the black hole interior during the merger. Based on this, our result suggests that the appearance of self-intersecting MOTS may be a far more general phenomenon than previously expected.

Initially we argued that the behaviour of MOTOS should constrain the possible evolution of MOTS during a black hole merger. This expectation was borne out by the sufficient variability we found in the behaviour of MOTOS to reproduce known evolution [39, 46, 47] for MOTS during black hole mergers. We went further and speculated about the possible behaviours that could be observed beyond what is previously known in the merging process. However, this suffers from the problem that we have been unable to pin down the correct surfaces in the right sequential order. This is due to a lack of clarity in the correct boundary conditions at infinity for the MOTOS. Another interesting approach is to evolve a correct initial MOTS in time in order to find a marginally outer trapped tube (MOTT) to understand the evolution. To achieve this, one has to solve complex partial differential evolution equations, which is beyond the scope of this work.

Considering the first case of the self-intersecting surfaces, there remain a number of future directions to be explored. Is rotational symmetry essential to the existence of self-intersecting surfaces? Do all black holes exhibit similar behaviour? What are the critical parameters for this behaviour? The second point concerns the relevance of the results to EMR mergers. Assuming that evolution of MOTS during EMR mergers can be approximated by the behaviours of MOT(O)S in Schwarzschild geometry, how do we choose the correct surfaces with correct order? As mentioned previously the other way to do it is to solve partial differential equations for MOTT. Even if we able to do so, how do we choose the correct initial surface to evolve? We expect to explore and try to answer these questions in future work.

Bibliography

[1] A. J. Amsel, D. Marolf, and A. Virmani. Collisions with black holes and deconfined plasmas. *Journal of High Energy Physics*, 2008(04):025–025, Apr 2008.

[2] L. Andersson, M. Mars, J. Metzger, and W. Simon. The time evolution of marginally trapped surfaces. *Classical and Quantum Gravity*, 26(8):085018, Apr 2009.

[3] A. Ashtekar, M. Campiglia, and S. Shah. Dynamical black holes: Approach to the final state. *Physical Review D*, 88(6), Sep 2013.

[4] A. Ashtekar and G. J. Galloway. Some uniqueness results for dynamical horizons. *Adv. Theor. Math. Phys.*, 9(1):1–30, 2005.

[5] A. Ashtekar and B. Krishnan. Dynamical horizons and their properties. *Physical Review D*, 68(10), Nov 2003.

[6] A. Ashtekar and B. Krishnan. Isolated and dynamical horizons and their applications. *Living Reviews in Relativity*, 7(1), Dec 2004.

[7] T. Baumgarte. Numerical relativity and compact binaries. *Physics Reports*, 376(2):41–131, Mar 2003.

[8] I. Ben-Dov. Penrose inequality and apparent horizons. *Physical Review D*, 70(12), Dec 2004.

[9] I. Bengtsson. Some examples of trapped surfaces, 2011.

[10] I. Booth. Black-hole boundaries. *Canadian Journal of Physics*, 83(11):1073–1099, Nov 2005.

[11] I. Booth. Two physical characteristics of numerical apparent horizons. *Canadian Journal of Physics*, 86(4):669–673, Apr 2008.

[12] I. Booth, L. Brits, J. A. Gonzalez, and C. V. D. Broeck. Marginally trapped tubes and dynamical horizons. *Classical and Quantum Gravity*, 23(2):413–439, Dec 2005.

[13] I. Booth, R. Hennigar, and S. Mondal. Marginally outer trapped (open) surfaces and extreme mass ratio mergers. *Phys. Rev. D*, 102(4):044031, 2020.

[14] R. Bousso and N. Engelhardt. Proof of a new area law in general relativity. *Physical Review D*, 92(4), Aug 2015.

[15] T. Chu, H. P. Pfeiffer, and M. I. Cohen. Horizon dynamics of distorted rotating black holes. *Physical Review D*, 83(10), May 2011.

[16] A. Einstein. Über einen die erzeugung und verwandlung des lichtes betreffenden heuristischen gesichtspunkt. *Annalen der Physik*, 322(6):132–148, 1905.

[17] R. Emparan and M. Martinez. Exact Event Horizon of a Black Hole Merger. *Class. Quant. Grav.*, 33(15):155003, 2016.

[18] R. Emparan, M. Martínez, and M. Zilhão. Black hole fusion in the extreme mass ratio limit. *Physical Review D*, 97(4), Feb 2018.

[19] R. Emparan and M. Martınez. Black string flow. *Journal of High Energy Physics*, 2013(9), Sep 2013.

[20] R. Emparan and D. Marín. Precursory collapse in neutron star-black hole mergers. *Physical Review D*, 102(2), Jul 2020.

[21] B. P. A. et al. Gw150914: The advanced ligo detectors in the era of first discoveries. *Phys. Rev. Lett.*, 116:131103, Mar 2016.

[22] B. P. A. et al. Observation of Gravitational Waves from a Binary Black Hole Merger. *Phys. Rev. Lett.*, 116:061102, Feb 2016.

[23] C. Evans, D. Ferguson, B. Khamesra, P. Laguna, and D. Shoemaker. Inside the final black hole: Puncture and trapped surface dynamics, 2020.

[24] P. Figueras, V. E. Hubeny, M. Rangamani, and S. F. Ross. Dynamical black holes and expanding plasmas. *Journal of High Energy Physics*, 2009(04):137–137, Apr 2009.

[25] E. Gourgoulhon and J. L. Jaramillo. Area evolution, bulk viscosity, and entropy principles for dynamical horizons. *Physical Review D*, 74(8), Oct 2006.

[26] A. Gupta, B. Krishnan, A. B. Nielsen, and E. Schnetter. Dynamics of marginally trapped surfaces in a binary black hole merger: Growth and approach to equilibrium. *Phys. Rev. D*, 97:084028, Apr 2018.

[27] R. Hamerly and Y. Chen. Event horizon deformations in extreme mass-ratio black hole mergers. *Physical Review D*, 84(12), Dec 2011.

[28] S. Hawking and R. Penrose. The Singularities of gravitational collapse and cosmology. *Proc. Roy. Soc. Lond. A*, A314:529–548, 1970.

[29] S. W. Hawking and G. F. R. Ellis. *The Large Scale Structure of Space-Time*. Cambridge Monographs on Mathematical Physics. Cambridge University Press, 1973.

[30] C. A. R. Herdeiro and J. P. S. Lemos. The black hole fifty years after: Genesis of the name, 2018.

[31] V. E. Hubeny, H. Maxfield, M. Rangamani, and E. Tonni. Holographic entanglement plateaux. *Journal of High Energy Physics*, 2013(8), Aug 2013.

[32] U. Hussain and I. Booth. Deformation of horizons during a merger. *Class. Quant. Grav.*, 35(1):015013, 2018.

[33] J. L. Jaramillo, M. Ansorg, N. Vasset, K. E. Kunze, M. Mars, and M. A. Vazquez-Mozo. Application of initial data sequences to the study of black hole dynamical trapping horizons. *AIP Conference Proceedings*, 2009.

[34] P.-S. Laplace. *Exposition du systéme du monde*. Cambridge Library Collection - Mathematics. Cambridge University Press, 2 edition, 2009.

[35] C. O. Lousto and R. H. Price. Understanding initial data for black hole collisions. *Phys. Rev. D*, 56:6439–6457, Nov 1997.

[36] K. Martel and E. Poisson. One-parameter family of time-symmetric initial data for the radial infall of a particle into a schwarzschild black hole. *Phys. Rev. D*, 66:084001, Oct 2002.

[37] J. Michell. On the Means of Discovering the Distance, Magnitude, &c. of the Fixed Stars, in Consequence of the Diminution of the Velocity of Their Light, in Case Such a Diminution Should be Found to Take Place in any of Them, and Such Other Data Should be Procured from Observations, as Would be Farther Necessary for That Purpose. By the Rev. John Michell, B. D. F. R. S. In a Letter to Henry Cavendish, Esq. F. R. S. and A. S. *Philosophical Transactions of the Royal Society of London Series I*, 74:35–57, Jan. 1784.

[38] J. D. Mollon. The origins of the concept of interference. *Philosophical Transactions: Mathematical, Physical and Engineering Sciences*, 360(1794):807–819, 2002.

[39] P. Mosta, L. Andersson, J. Metzger, B. Szilagyi, and J. Winicour. The merger of small and large black holes. *Classical and Quantum Gravity*, 32(23):235003, Dec 2015.

[40] A. B. Nielsen. Black holes and black hole thermodynamics without event horizons. *General Relativity and Gravitation*, 41(7):1539–1584, Jan 2009.

[41] R. Penrose. Conformal treatment of infinity. pages 565–586, 1964.

[42] R. Penrose. Gravitational collapse and space-time singularities. *Phys. Rev. Lett.*, 14:57–59, Jan 1965.

[43] R. Penrose. Gravitational collapse: The role of general relativity. *Riv. Nuovo Cim.*, 1:252–276, 1969.

[44] R. Penrose. Techniques of differential topology in relativity. 1972.

[45] E. Poisson. *A Relativist's Toolkit: The Mathematics of Black-Hole Mechanics*. Cambridge University Press, 2004.

[46] D. Pook-Kolb, O. Birnholtz, B. Krishnan, and E. Schnetter. Interior of a binary black hole merger. *Physical Review Letters*, 123(17), Oct 2019.

[47] D. Pook-Kolb, O. Birnholtz, B. Krishnan, and E. Schnetter. Self-intersecting marginally outer trapped surfaces. *Physical Review D*, 100(8), Oct 2019.

[48] T. Sauer. Chapter 63 - albert einstein, review paper on general relativity theory (1916). In I. Grattan-Guinness, R. Cooke, L. Corry, P. Crépel, and N. Guicciardini, editors, *Landmark Writings in Western Mathematics 1640-1940*, pages 802 – 822. Elsevier Science, Amsterdam, 2005.

[49] E. Schnetter and B. Krishnan. Nonsymmetric trapped surfaces in the schwarzschild and vaidya spacetimes. *Physical Review D*, 73(2), Jan 2006.

[50] E. Schnetter, B. Krishnan, and F. Beyer. Introduction to dynamical horizons in numerical relativity. *Physical Review D*, 74(2), Jul 2006.

[51] K. Schwarzschild. On the gravitational field of a mass point according to einstein's theory, 1999.

[52] J. M. M. Senovilla. Singularity theorems and their consequences. *General Relativity and Gravitation*, 30(5):701–848, May 1998.

[53] J. M. M. SENOVILLA. Trapped surfaces. *International Journal of Modern Physics D*, 20(11):2139–2168, Oct 2011.

[54] A. Spallicci. Free fall and self-force: An historical perspective. *Fundam. Theor. Phys.*, 162:561–603, 2011.

[55] M. Sun and Y.-C. Huang. Kerr black string flow. *Nuclear Physics B*, 897:98–110, Aug 2015.

[56] B. Szilágyi, D. Pollney, L. Rezzolla, J. Thornburg, and J. Winicour. An explicit harmonic code for black-hole evolution using excision. *Classical and Quantum Gravity*, 24(12):S275–S293, Jun 2007.

[57] J. Thornburg. Event and apparent horizon finders for 3+1 numerical relativity, 2005.

[58] R. M. Wald. *General Relativity.* Chicago Univ. Pr., Chicago, USA, 1984.

[59] F. J. Zerilli. Gravitational field of a particle falling in a schwarzschild geometry analyzed in tensor harmonics. *Phys. Rev. D*, 2:2141–2160, Nov 1970.

[60] J. Ziprick and G. Kunstatter. Numerical study of black-hole formation in painlevé-gullstrand coordinates. *Physical Review D*, 79(10), May 2009.